The Astronomical Journal, 144:23 (24pp), 2012 July doi:10.1088/0004-6256/144/1/23

THE RESONANT TRANS-NEPTUNIAN POPULATIONS*

B. Gladman[1], S. M. Lawler[1], J.-M. Petit[2], J. Kavelaars[3], R. L. Jones[4], J. Wm. Parker[5], C. Van Laerhoven[1], P. Nicholson[6], P. Rousselot[2], A. Bieryla[5,7], and M. L. N. Ashby[7]
[1] Department of Physics & Astronomy, 6224 Agricultural Road, University of British Columbia, Vancouver, BC V6T 1Z1, Canada
[2] Institut UTINAM, CNRS-UMR 6213, Observatoire de Besançon, BP 1615, 25010 Besançon Cedex, France
[3] Herzberg Institute of Astrophysics, National Research Council of Canada, Victoria, BC V9E 2E7, Canada
[4] Department of Astronomy, University of Washington, Seattle, WA 98195, USA
[5] Southwest Research Institute, 1050 Walnut Street, Suite 300, Boulder, CO 80302, USA
[6] Department of Astronomy, Cornell University, Ithaca, NY 14853, USA
[7] Harvard-Smithsonian Center for Astrophysics, 60 Garden Street, Cambridge, MA 02138, USA
Received 2011 July 18; accepted 2012 May 10; published 2012 June 12

ABSTRACT

The trans-Neptunian objects (TNOs) trapped in mean-motion resonances with Neptune were likely emplaced there during planet migration late in the giant-planet formation process. We perform detailed modeling of the resonant objects detected in the Canada–France Ecliptic Plane Survey (CFEPS) in order to provide population estimates and, for some resonances, constrain the complex internal orbital element distribution. Detection biases play a critical role because phase relationships with Neptune make object discovery more likely at certain longitudes. This paper discusses the 3:2, 5:2, 2:1, 3:1, 5:1, 4:3, 5:3, 7:3, 5:4, and 7:4 mean-motion resonances, all of which had CFEPS detections, along with our upper limit on 1:1 Neptune Trojans (which is consistent with their small population estimated elsewhere). For the plutinos (TNOs in the 3:2 resonance) we refine the orbital element distribution given by Kavelaars et al. in 2009 and show that steep H-magnitude distributions ($N(H) \propto 10^{\alpha H}$, with $\alpha = 0.8$–0.9) are favored in the range $H_g = 8$–9, and confirm that this resonance does not share the inclination distribution of the classical Kuiper Belt. We give the first population estimate for the 5:2 resonance and find that, to within the uncertainties, the population is equal to that of the 3:2 ($\simeq$13,000 TNOs with $H_g < 9.16$), whereas the 2:1 population is smaller by a factor of 3–4 compared to the other two resonances. We also measure significant populations inhabiting the 4:3, 5:3, 7:3, 5:4, 7:4, 3:1, and 5:1 resonances, with $H_g < 9.16$ ($D > 100$ km) populations in the thousands. We compare our intrinsic population and orbital element distributions with several published models of resonant-TNO production; the most striking discrepancy is that resonances beyond the 2:1 are in reality more heavily populated than in published models.

Key words: celestial mechanics – Kuiper Belt: general

Online-only material: color figures

1. INTRODUCTION

The resonant trans-Neptunian objects (TNOs) are a set of Edgeworth–Kuiper Belt objects whose orbital elements are such that the perturbations of Neptune causes relatively large-amplitude ($\sim$1%) oscillations of the orbit on only 10^4 yr timescales (much faster than secular oscillations in the outer solar system). A necessary but not sufficient condition for an object to be in a mean-motion resonance is that its semimajor axis a implies an orbital period P which is a low-order integer ratio with Neptune with $P/P_N \simeq j/k$, where j and k are two small integers, in which case the object is said to be in the j:k resonance[8] with Neptune, whose period is P_N and semimajor axis a_N. Kepler's third law then provides the resonant semimajor axis $a = a_N(P/P_N)^{2/3}$. Pluto was the first known resonant TNO; its presence in the 3:2 resonance at $a \simeq 39.5$ AU was discovered via direct numerical integration (Cohen & Hubbard 1965). An important property of these resonances is that even resonant TNOs with eccentricities e so high that their perihelia q satisfy $q = a(1-e) < a_N$, and thus approach the Sun more closely than Neptune, are "phase protected" by the resonance due to Neptune never being nearby when the TNO is at pericenter; in the case of Pluto, this phase protection means the planet actually gets closer to Uranus than Neptune (although Pluto's orbit is especially rich in resonant behaviors; Milani et al. 1989).

In less than a year after the first moderately sized TNOs began to be discovered in the 1990s, other TNOs in the 3:2 resonance were recognized (Davies et al. 2008). Termed "plutinos" (Jewitt & Luu 1995), these objects remain the most numerous of the known resonant objects, with Davies et al. (2008) reviewing the historical recognition of TNOs in other resonances. The most recent compilations of accurately measured resonant orbits (Gladman et al. 2008; Lykawka & Mukai 2007) list objects from the 1:1 (Trojan) resonance all the way out to the 27:4 for 2004 $PB_{112} = I4212$ as the current record holder for the largest resonant TNO semimajor axis, at $\simeq$108 AU. It is likely that even larger-a resonant TNOs exist, but because the high-order resonances are thin in phase space, extremely accurate orbits are required before the resonant behavior can be confirmed.

A powerful idea is that the resonant TNOs were captured during an outward migration of Neptune in the distant past, although there exist several contexts. Malhotra (1993) proposed Pluto's eccentricity had its origin due to capture into the 3:2 as

* Based on observations obtained with MegaPrime/MegaCam, a joint project of CFHT and CEA/DAPNIA, at the Canada–France–Hawaii Telescope (CFHT) which is operated by the National Research Council (NRC) of Canada, the Institute National des Sciences de l'Universe of the Centre National de la Recherche Scientifique (CNRS) of France, and the University of Hawaii. This work is based in part on data products produced at the Canadian Astronomy Data Centre as part of the Canada–France–Hawaii Telescope Legacy Survey, a collaborative project of NRC and CNRS.

[8] The literature is mixed as to whether the periods or the mean-motions should be the integer ratio, and thus some would call the external resonance with twice Neptune's orbital period the 1:2 resonance.

the resonance swept over the initial heliocentric orbit of Pluto during Neptune's outward migration; after capture, Neptune's continued migration forced up the captured TNO's e due to conservation of angular momentum. Hahn & Malhotra (2005) explored the sweep-up of resonant objects into a variety of resonances, showing how models match the observed-TNO distribution better if the resonances migrated into a primordial belt that has already been dynamically heated rather than the $e \sim i \sim 0$ case of a dynamically cold planetesimal disk, although achieving an inclination i distribution as hot as the observed objects was difficult. Gomes (2003) showed that abundant large-i plutinos could be produced if the plutinos were trapped out of a scattering disk already having interacted with Neptune, rather than from a pre-existing cold belt. Chiang & Jordan (2002), Chiang et al. (2003), and Murray-Clay & Chiang (2005) simulated resonant capture, looking at the population of resonances after the migration phase, including studying how the relative populations of resonant "modes" in the 2:1 resonance varied as a function of Neptune's migration distance and rate. All these studies identified the problem that even though these models pump eccentricities via the capture process, they still favored migration into a dynamically pre-heated disk and even then the inclination distribution of the trapped resonant objects is not sufficiently high. More recently, Levison et al. (2008) explored the idea that the *entire Kuiper Belt* was "planted" in its current location as particles scattering off of Neptune during the late stages of planet formation[9] are dropped to lower eccentricity while temporarily trapped in mean-motion resonance, and are then decoupled into the current Kuiper Belt; in this model the resonant particles are simply those that remained in the resonances at the end of migration. This model has several desirable properties, although the production of a Kuiper Belt with the correct inclination distribution is a challenge (Petit et al. 2011). In our present manuscript, we will compare our measurements of how various resonances are populated with some published models.

1.1. Resonance Dynamics

We provide only a brief tutorial on TNO resonant dynamics; further introductory material can be found in Morbidelli et al. (1995), Malhotra (1996), Chiang & Jordan (2002), and Gladman & Kavelaars (2009).

Many TNOs are currently known to be in mean-motion resonances with Neptune,[10] meaning that the TNO's orbit is coupled to that of Neptune. Neptune's mean longitude λ_N (roughly its location around its orbit as measured from the J2000 ecliptic reference axis) is related to the TNO's longitude λ (its current position) and the longitude ϖ of where the TNO's perihelion location is located. Operationally, inhabiting the j:k resonance can be diagnosed by confirming (in a numerical integration) that the resonant angle

$$\phi_{jk} = j\lambda - k\lambda_N - (j-k)\varpi \quad (1)$$

does not explore all values from 0° to 360°. The most common case (but not only possibility) for real resonant TNOs is that ϕ_{jk} oscillates (librates) around a mean $\langle\phi_{jk}\rangle = 180°$ with some amplitude L_{jk} (termed the libration amplitude). For example, a TNO in the 7:4 resonance with libration amplitude $L_{74} = 10°$ means that ϕ_{74} oscillates (roughly sinusoidally) between 170° and 190°; such small amplitudes are rare in reality. Because $\lambda = \varpi + \mathcal{M}$ where $\mathcal{M}$ is the TNO's mean anomaly, Equation (1) forces that when the TNO is at perihelion ($\mathcal{M} = 0$),

$$\varpi - \lambda_N = \frac{1}{k}\,\phi_{jk}. \quad (2)$$

In our example of the 7:4 resonance, this means that the TNO's pericenter is "leading" ($\varpi - \lambda_N$) Neptune by $(180°/4) = 45°$ for $\langle\phi_{74}\rangle = 180°$; as ϕ_{74} oscillates by ±10°, the perihelion longitude oscillates by $(10°/4) = 2.°5$ relative to the 45° offset (see the first panel of Figure 1). Because $\phi_{74} = 540°$, 900°, and 1260° (adding multiples of 360° to 180°) are all also valid, this results in perihelion longitudes for libration center to be 45°, 135°, 225°, and 315° ahead of Neptune for $L_{74} = 0°$ TNOs; essentially one can add $2\pi m/k$ for any integer m to the right-hand side of Equation (2). It is instructive to "trace the orbit" of a single low-libration-amplitude TNO in the corotating panels of Figure 1; any single particle for the j:k resonance explores all k perihelion concentrations after making k orbits around the Sun. During that time Neptune will have made j heliocentric orbits.

The two rightmost panels of Figure 1 illustrate the different generic case of the n:1 resonances, which can librate in more that one state of perihelion locking relative to Neptune (these are usually called different "islands") despite the fact that $k = 1$ in Equation (2). Although these resonances still have "symmetric" libration of the resonant argument ϕ_{n1} around an average value of $\langle\phi_{n1}\rangle = 180°$, usually with very large amplitude, they can also exhibit "asymmetric libration" around another $\langle\phi_{n1}\rangle$ which depends on the value of the orbital eccentricity (Beauge 1994; Malhotra 1996). Because these are n:1 resonances, the perihelion location of such a given particle is confined to one of the two sky longitudes (hence the term asymmetric); if the reader traces an asymmetric 3:1 orbit in Figure 1 they will see that it does *not* visit both perihelion clusters.

The existence of confined pericenter locations for resonant TNOs has important implications for their observational study; surveys are most sensitive to resonant TNOs that can be at perihelion in the patch of sky being examined. Because the number of TNOs increases rapidly as one goes to fainter magnitudes (due to the size distribution being steep) and because most resonant TNOs occupy eccentric orbits ($e > 0.1$ or much larger), the number of detectable TNOs above the limit of a flux-limited survey is a strong function of longitude relative to Neptune. Essentially one becomes dominated by the hordes of smaller TNOs present near perihelion that become the majority of a detected sample. Although this is a generic effect of eccentric populations (Jones et al. 2006), it is more severe for the resonant populations than the main classical belt due to the usually lower eccentricities of the latter; we will illustrate this effect below with the plutino population. The longitude bias in ϖ shown in Figure 1's toy models are more extreme than reality because the libration-amplitude distribution of the resonances is not concentrated toward zero. This introduces yet another effect: during the oscillation of the resonant argument more time passes with ϕ_{jk} near the extremes

$$\left|\phi_{jk}\right|_{\rm extremal} = \langle\phi_{jk}\rangle \pm L_{jk} \quad (3)$$

than at the libration center $\langle\phi_{jk}\rangle$ itself. As an example, using the 5:3 resonance (Figure 1), if one were looking 85° ahead of

[9] The Levison et al. (2008) simulations are done in the context of the Nice model, which is usually stated to be occurring 600 Myr after solar system formation. However, the Kuiper Belt implantation physics would work just as well if the outward migration occurred in the few Myr following planetary formation.

[10] No TNOs are yet securely known to inhabit mean-motion resonances with any other planets.

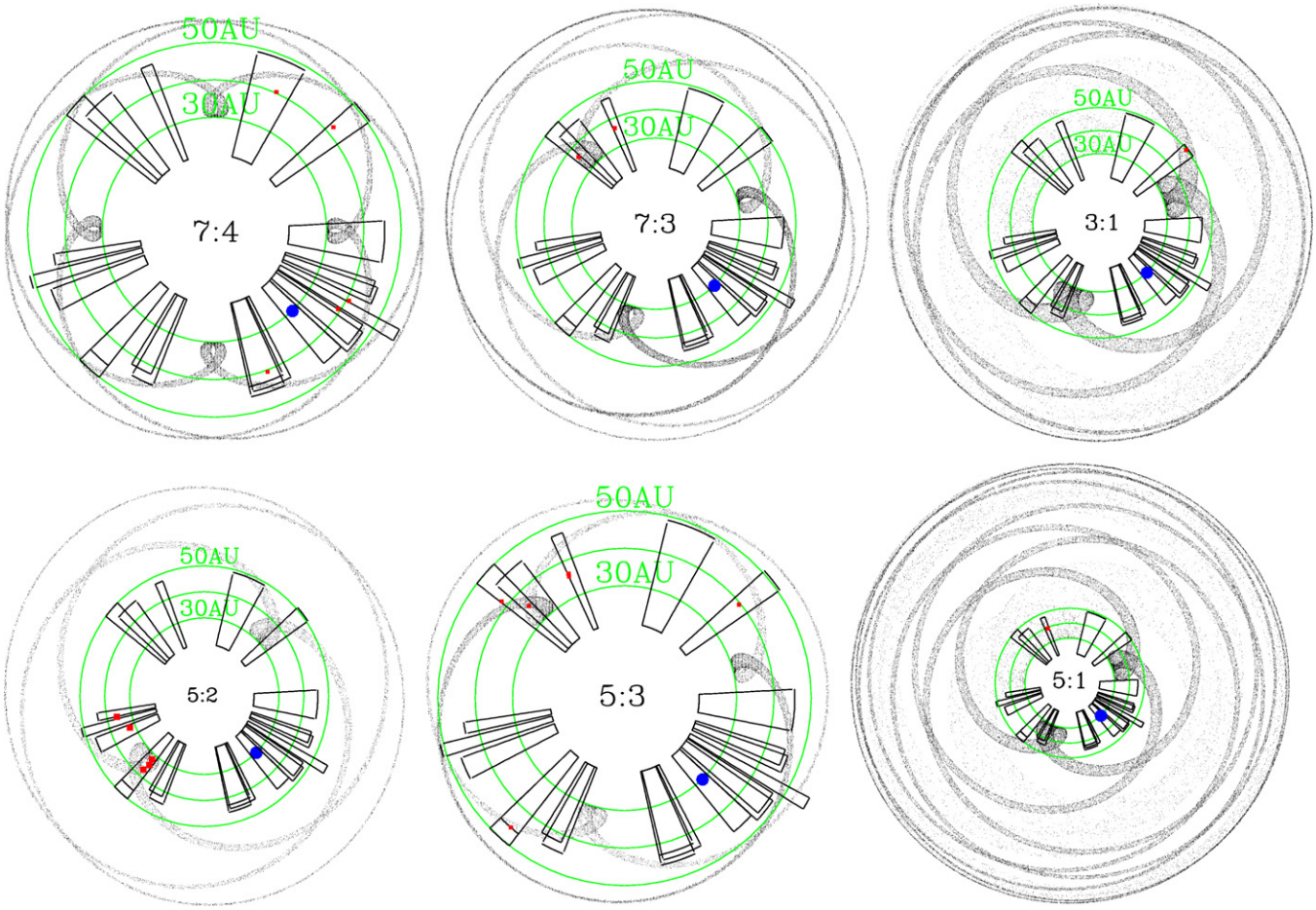

Figure 1. Toy models giving ecliptic projections (black dots) of TNOs with $i \simeq 0°$, $q \simeq 30$ AU, and libration amplitudes of 10°, to illustrate basic spatial TNO distribution induced by a given resonance. These patterns stay fixed in the frame that corotates with Neptune, whose position is indicated by the large blue dot; green reference circles show heliocentric distances of $d = 30$, 40, and 50 AU. Wedges show the ecliptic longitude range of the CFEPS blocks (labeled in Figure 2), and red squares show the locations of the real CFEPS TNOs in that resonance. For the 3:1 and 5:1, 10% of the model objects are in the symmetric libration island (with 50° libration amplitudes) and 45% in each of the two asymmetric islands (with 10° amplitudes).

(A color version of this figure is available in the online journal.)

Neptune, then the 5:3 resonators (from the nearby "average" $\langle \phi_{53} \rangle = 60°$ perihelion cluster) with $L_{53} \simeq 75°$ ($k = 3$ times larger than the 25° longitude difference, cf. Equation (2)) will be favored over other 5:3 resonators, if all other parameters are equal.

A similar detection bias is caused by orbital inclination i; as a TNO rises and falls in ecliptic latitude it will spend less time at latitudes near the ecliptic than at latitudes close to $\pm i$. This results in the true intrinsic TNO sky density of a given inclination peaking just below the latitude corresponding to the inclination, and the ecliptic being the least likely place to find any given high-i TNO.

The real population in any given resonance is a superposition of all eccentricities, libration centers, and libration amplitudes. Conclusions about the distribution of any of these parameters cannot be quantitative without detailed understanding of the longitude coverage and depth of the surveys in which they were found.

2. RESONANT CFEPS OBJECTS

The data acquisition of the Canada–France Ecliptic Plane Survey (CFEPS) is described elsewhere (Jones et al. 2006; Kavelaars et al. 2009; Petit et al. 2011). The survey coverage was divided into "blocks" of contiguous sky around the ecliptic, labeled L3f through L7a, where the number indicates the calendar year of the block's "discovery" observations (2003 through 2007) and the letter is the common Minor Planet Center (MPC) format designation of the two-week chunk to the calendar year (thus, discovery observations of L5c were performed in the first half of 2005 February). Objects discovered in the block are given internal designations like L5c11, indicating the eleventh TNO discovered in the L5c block.

This paper models the resonant CFEPS TNOs that are characterized detections[11] from the 3:2 (Plutinos) and 5:2 resonances, three n:3 resonances (the 4:3, 5:3, and 7:3), the 5:4 and 7:4 resonance, and three n:1 resonances (the 2:1, 3:1, and 5:1). The orbital elements for the CFEPS TNOs in these resonances are given in Tables 1 and 2. In addition, we give a 95% confidence upper limit on the Neptune Trojan population from our non-detection of such an object. Other resonances had zero or one CFEPS TNOs in them, and we elected to not generate upper limits on their populations.

The discovery and tracking of these objects is discussed in Petit et al. (2011). Important for our purposes here is: (1) a wide range of ecliptic longitudes were surveyed with CFEPS,

[11] Characterized detections are those which have detection efficiencies >40% in their CFEPS discovery block, as defined in Jones et al. (2006).

Table 1
CFEPS 3:2 (Plutinos) and 5:2 Resonators

Designations		a	e	i	d	Res	Amp	Mag	Comment
CFEPS	MPC	(AU)		(°)	(AU)		(°)	(g)	.
L4k11	2004 KC19	39.258	0.23605	5.637	30.2	3:2	79 ± 23	23.3	
L4h15	2004 HB79	39.260	0.22862	2.661	32.0	3:2	82 ± 13	24.0	
L5c11	2005 CD81	39.262	0.15158	21.344	45.2	3:2	98 ± 7	23.7	
L4h06	2004 HY78	39.302	0.19571	12.584	31.8	3:2	74 ± 8	23.8	
L4v18	2004 VY130	39.342	0.27616	10.203	28.5	3:2	38 ± 19	23.3	
L4m02	2004 MS8	39.344	0.29677	12.249	27.8	3:2	125 ± 2	23.4	
L3s02	2003 SO317	39.346	0.2750	6.563	32.3	3:2	100 ± 20	23.8	
L4h09PD	47932	39.352	0.28120	10.815	28.5	3:2	54 ± 15	21.3	
L3h19	2003 HF57	39.36	0.194	1.423	32.4	3:2	60 ± 20	24.2	
L3w07	2003 TH58	39.36	0.0911	27.935	35.8	3:2	100 ± 10	23.0	
L4h07	2004 HA79	39.378	0.24697	22.700	38.4	3:2	46 ± 11	23.7	Kozai $270° \pm 30°$
L3h11	2003 HA57	39.399	0.1710	27.626	32.7	3:2	70 ± 5	23.4	
L3w01	2005 TV189	39.41	0.1884	34.390	32.0	3:2	60 ± 20	22.9	
L4j11	2004 HX78	39.420	0.15270	16.272	33.6	3:2	28 ± 5	23.6	
L4v09	2004 VX130	39.430	0.20696	5.745	34.8	3:2	50 ± 32	23.5	
L3h14	2003 HD57	39.44	0.179	5.621	32.9	3:2	60 ± 30	23.3	
L3s05	2003 SR317	39.44	0.1667	8.348	35.5	3:2	90 ± 5	23.7	
L4v13	2004 VV130	39.454	0.18827	23.924	32.8	3:2	49 ± 12	22.7	
L4k01	2004 KB19	39.484	0.21859	17.156	39.5	3:2	57 ± 31	24.0	Kozai $270° \pm 50°$
L3h01	2004 FW164	39.492	0.1575	9.114	33.3	3:2	80 ± 20	23.8	
L5i06PD	2001 KQ77	39.505	0.15619	15.617	36.2	3:2	72 ± 8	23.1	
L4h10PD	1995 HM5	39.521	0.25197	4.814	31.1	3:2	77 ± 20	23.8	
L4v12	2004 VZ130	39.551	0.28159	11.581	29.2	3:2	88 ± 10	24.0	
L4h08	2004 HZ78	39.580	0.15095	13.310	34.8	3:2	115 ± 15	23.0	
L4j08	2004 HO79	55.206	0.41166	5.624	37.3	5:2	84 ± 20	23.5	
L3f04PD	60621	55.29	0.4020	5.869	36.0	5:2	80 ± 30	22.7	
L4j06PD	2002 GP32	55.387	0.42195	1.559	32.1	5:2	65 ± 2	22.1	
L4k14	2004 KZ18	55.419	0.38191	22.645	34.4	5:2	44 ± 10	24.1	
L4h02PD	2004 EG96	55.550	0.42291	16.213	32.2	5:2	91 ± 17	23.5	

Notes. Characterized CFEPS resonators, with MPC (where available) designations. A "PD" suffix indicates that the CFEPS team realized immediately that this was a previously discovered TNO, but which could now be used in our flux-calibrated analysis. All digits in the best-fit barycentric orbital $a/e/i$ are significant. g-band magnitudes are rounded to 0.1 mag, with exact values and errors given in Table 7 of Petit et al. (2011). Heliocentric distances d and H_g magnitudes are given at the first date of CFEPS detection. Libration amplitude is the best-fit orbit's value along with the range covering >99% of possible values given orbital uncertainties. For Kozai librators the libration center of ω and amplitude A_ω are given.

which means CFEPS was sensitive to objects with a large variety of libration amplitudes, (2) patches of sky away from the perihelion longitudes of the resonances were quantitatively characterized; the *non-detection* of resonant objects at those longitudes provides powerful constraints on the large-amplitude resonators, and (3) an extremely high fraction of the discoveries were tracked, preventing loss of unusual objects, as described in Jones et al. (2010). As an example of this, CFEPS re-discovered TNOs actually inhabiting the rare 5:4 and 7:3 mean-motion resonances (L3y11, L3y07, and L5c19PD; see Table 2 caption) at on-sky positions $\sim 1°$ from the ephemeris that had been assigned based on an incorrect orbit computed from the short-arc discovery prior to 2003 (i.e., the TNOs had been lost before their resonant nature was recognized).

Tables 1 and 2 list the current barycentric a, e, i J2000 osculating elements of each object and a determination of the resonant libration amplitude, which comes from the range of possible orbits as diagnosed in the method of Gladman et al. (2008). The resonance amplitudes listed should be interpreted as a range which encompasses nearly all (>99%) of the possible true values of the TNO's libration amplitude. Because the CFEPS tracking strategy regularly provided off-opposition observations during the three-opposition orbits, the libration amplitudes for the CFEPS sample are more precise than for the majority of the MPC sample given in Gladman et al. (2008) and Lykawka & Mukai (2007) because many of the objects in the MPC database have much sparser astrometric coverage.

In addition to mean-motion libration amplitudes, the Kozai resonance (see the Appendix) is observed to function for two CFEPS plutinos (L4h07 and L4k01); Table 1 gives the amplitude and mean value of the argument of pericenter ω (which is effectively the resonant angle). For objects in n:1 resonances where there are symmetric and asymmetric libration islands, Table 2 identifies the mode and estimates of the libration center position and libration amplitude.

There are a few high-order resonances with CFEPS detections which we do not model here due to the fact that the resonant occupation is not yet secure. These include the 15:8, 17:9, and 12:5 mean-motion resonances, and are listed as insecure resonators in Petit et al. (2011).

3. CFEPS SURVEY SIMULATION OF A RESONANT POPULATION

We model the orbital distribution in each resonance with several goals. The orbital element distribution inside each resonance is represented either by a parametric model or, in the case of the n:1 resonances, a prescription based on the known dynamics of the resonance. In the case of a parametric model, the functional forms chosen are ones which post-facto provide a

Table 2
CFEPS TNOs in Resonances Other than 3:2 and 5:2

Designations		a	e	i	d	Res	Amp	Mag	Comment
CFEPS	MPC	(AU)		(°)	(AU)		(°)	(g)	.
L3y11	131697	34.925	0.0736	2.856	34.0	5:4	75 ± 5	23.8	MPC_W
L4h14	2004 HM79	36.441	0.07943	1.172	38.0	4:3	63 ± 1	23.7	
L3s06	143685	36.456	0.2360	5.905	28.2	4:3	60 ± 20	22.8	
L5c23	2005 CF81	36.473	0.06353	0.405	34.4	4:3	47 ± 15	24.2	
L7a10	2005 GH228	36.663	0.18814	17.151	30.6	4:3	∼120	23.6	Insecure
L5c08	2006 CJ69	42.183	0.22866	17.916	35.5	5:3	70 ± 40	23.6	
L3y06	2003 YW179	42.193	0.1537	2.384	35.7	5:3	100 ± 20	23.7	
L5c13PD	2003 CX131	42.240	0.23387	9.757	41.8	5:3	72 ± 3	23.8	
L4v05	2004 VE131	42.297	0.25889	5.198	39.6	5:3	81 ± 31	24.1	
L3y12PD	126154	42.332	0.14043	11.078	36.4	5:3	100 ± 10	21.7	
L4k10	2004 KK19	42.410	0.14391	4.485	46.0	5:3	∼125	24.4	Insecure
L3q08PD	135742	43.63	0.125	5.450	40.7	7:4	∼60	23.7	
L4n03	2004 OQ15	43.646	0.12472	9.727	40.5	7:4	∼60	23.7	
L3w03	2003 YJ179	43.66	0.0794	1.446	40.3	7:4	∼130	23.8	
L4v10	2004 VF131	43.672	0.21492	0.816	42.0	7:4	∼90	23.9	
K02O03	2000 OP67	43.72	0.191	0.751	39.3	7:4	∼70	24.3	
L4h18	2004 HP79	47.567	0.18250	2.253	39.5	2:1	∼50	23.3	Asym. ∼258
L4k16	2004 KL19	47.660	0.32262	5.732	32.3	2:1	20 ± 7	24.0	Asym. 288 ± 1
L4k20	2004 KM19	47.720	0.29180	1.686	33.8	2:1	12 ± 4	23.8	Asym. 287 ± 1
K02O12	2002 PU170	47.75	0.2213	1.918	47.2	2:1	154 ± 4	24.3	Symm.
L4v06	2004 VK78	47.764	0.33029	1.467	32.5	2:1	23 ± 5	23.7	Asym. 73 ± 1
L3y07	131696	52.92	0.3221	0.518	36.6	7:3	100 ± 20	23.4	MPC_W
L5c19PD	2002 CZ248	53.039	0.38913	5.466	36.2	7:3	84 ± 20	23.8	MPC_W
L4v08	2004VD130	62.194	0.42806	8.024	49.7	3:1	∼160	24.0	Symmetric?
L3y02	2003 YQ179	88.38	0.5785	20.873	39.3	5:1	∼160	23.4	Insecure, symmetric

Notes. Characterized CFEPS and MPC (where available) designations are given; objects beginning with "K" are from the CFEPS presurvey (Jones et al. 2006). All digits in the best-fit barycentric J2000 orbital $a/e/i$ are significant. Heliocentric distances d at detection are rounded to 0.1 AU. g-band magnitudes are rounded to 0.1 mag, with exact values and errors given in Table 7 of Petit et al. (2011) or Jones et al. (2006) (the latter assuming $g-R = 0.8$). Libration amplitudes are the range covering >99% of possible true orbits. For n:1 resonances the libration island and mean-resonant argument are given. "Insecure" indicates that this resonance occupation is not secure according to the Gladman et al. (2008) criterion. "MPC_W" indicates the TNO was in MPC database with the wrong orbit; CFEPS re-found the objects (usually >1° from predicted location) and CFEPS discovery and tracking observations improved the orbit to the listed values.

reasonable match between the simulated and real CFEPS detections. In order to converge to our best models, candidate orbital distributions were tested as described in Kavelaars et al. (2009) and the best-matching models were determined; briefly, models for which one of the e, i, d, m_g, or L cumulative distributions have an Anderson–Darling statistic which occurs by random <5% of the time are rejected. For example, we find that for most of the resonances the intrinsic eccentricity distribution can be satisfactorily represented by a probability distribution in the form of a Gaussian with center at eccentricity e_c and half-width e_w (rejecting negative eccentricities). These parametric representations are entirely empirical, due to the fact that there is no physical model that provides a parametric form. However, because these functional forms provide rather satisfactory matches to the CFEPS detections, theoretical models of resonant-TNO production will have to provide orbital parameter distributions that give roughly the same distribution as our intrinsic model, rather than values in the biased MPC sample. For example, we find the plutino eccentricity distribution is strongly peaked near $e_c = 0.18$ with narrow width; this intrinsic $e_c = 0.18$ peak is below the median plutino e of 0.22 in the MPC. Similarly, we find the median intrinsic plutino inclination to be ≈16°, whereas detected samples from ecliptic surveys (biased toward low-inclination detections) have median inclinations ∼12° both for CFEPS and the Deep Ecliptic Survey (abbreviated DES hereafter; Gulbis et al. 2010).

Our second goal is to produce debiased population estimates for each resonance, in order to compare the resonances to each other and to other Kuiper Belt components. For many resonances we lack sufficient detected numbers to explore the internal orbital distribution in detail, but can nevertheless provide calibrated absolute population estimates which should be accurate to a factor of a few, based on analytic expectations of the resonance's internal structure,

The CFEPS Survey Simulator begins with synthetic objects having a range of H_g magnitudes and with orbital elements that place them within a given resonance, correctly time weighted for their occupation of different regions of phase space. Due to differing structure, orbital elements for each resonance's simulated objects are chosen differently; the procedures for each of the three groups of resonances are described in the Appendix. As each synthetic object is created, the CFEPS pointings, magnitude limits, and tracking efficiencies are applied to decide whether or not the object is detected. New synthetic objects are created and checked for detectability until a user-defined number of synthetic detections are acquired. If this desired number is equal to the number of CFEPS detections, the simulation provides an estimate of the intrinsic population of the resonance. If instead a cosmogonic model is available, a large number of synthetic detections may be requested, in order to build a well-sampled distribution of the orbital elements that the cosmogonic model predicts CFEPS should detect. The

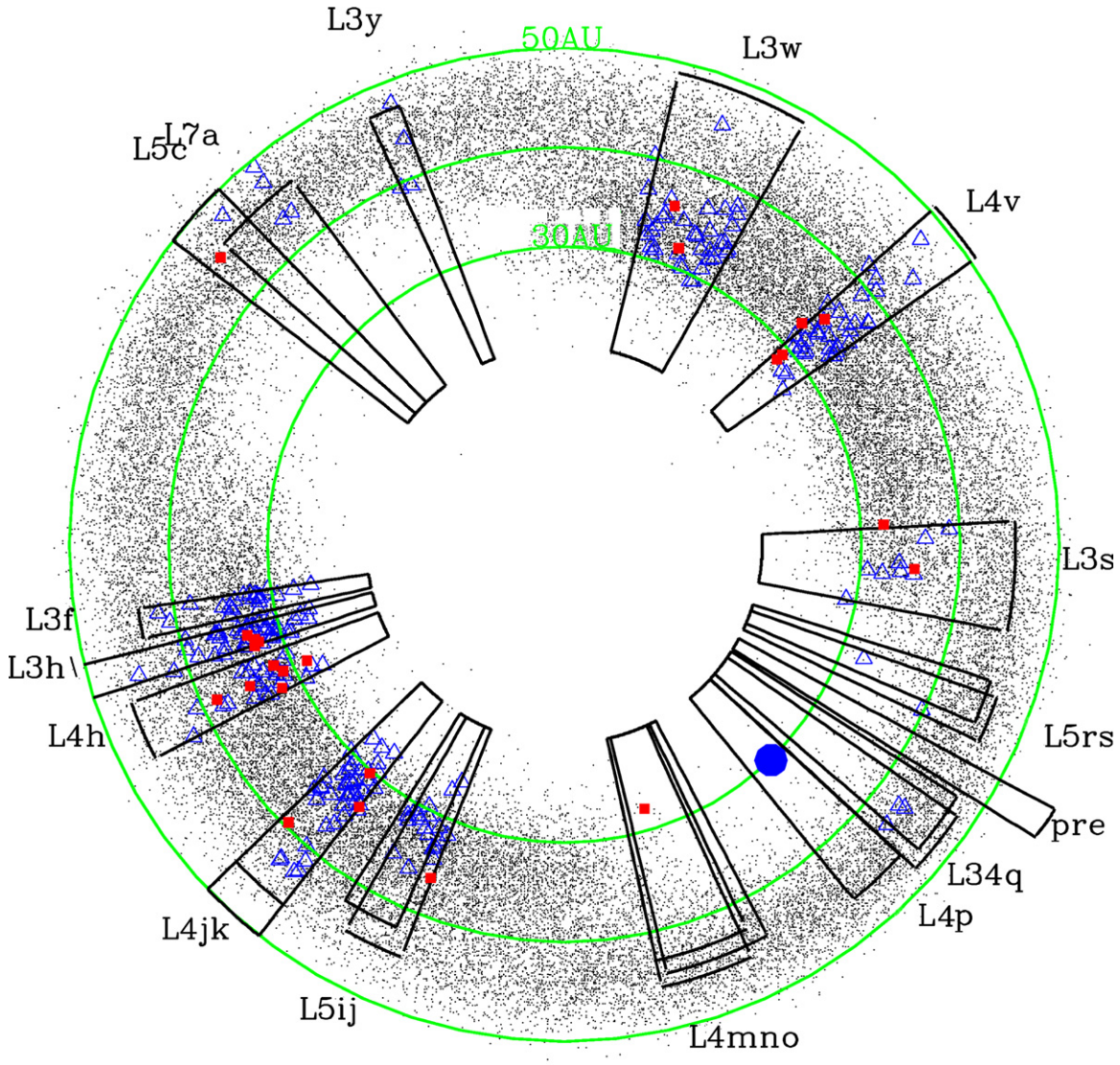

Figure 2. Ecliptic projection of the plutinos. The filled red squares are the 24 real detected plutinos, open blue triangles are 240 simulated detections, and tiny black dots show our model's intrinsic plutino distribution. Neptune's position is shown by the large blue dot. The CFEPS "blocks" are shown as wedges covering the correct ecliptic longitude range, where the inner edges at ∼20 AU are set by the detection pipeline's rate cut and the outer extent is at the distance where an $H_g = 7.5$ TNO would cease to be visible (larger TNOs are visible further away of course). The syntax L4jk means the L4j and L4k blocks are overlapping. The two ecliptic intersections with the galactic plane are roughly straight up and down in this diagram.

(A color version of this figure is available in the online journal.)

orbital elements (eccentricity, inclination, discovery distance, apparent magnitude, and libration amplitude) of these synthetic detections are then compared statistically to the real detections to determine whether or not our distribution of synthetic detections from that model is rejectable.

4. THE PLUTINOS (3:2 RESONATORS)

The plutinos (3:2 mean-motion librators) are by far the largest sample in the flux-biased catalogs. This preponderance is partly due to the low semimajor axis, keeping heliocentric distances d low, but detection of objects in n:2 resonances is also favored over many other resonances because their perihelion sky densities are currently (due to Neptune's position over the last two decades) larger at the high galactic latitudes that Kuiper Belt surveys have tended to favor. This well-known effect is illustrated in Figure 2 which shows the CFEPS survey block locations along with the CFEPS plutinos discovered (and tracked to obtain orbits with $\delta a/a < 10^{-4}$).

We began by improving the nominal CFEPS L3 plutino model, using the tripled sample size of 24 CFEPS detections (8 of which were part of the L3 plutino sample). To our surprise, the orbital distribution settled on by Kavelaars et al. (2009) from only eight characterized L3 plutinos remains a non-rejectable model despite tripling the sample, showcasing the ability of well-characterized surveys to constrain orbital distributions. Although we cannot reject the L3 plutino model, the 24 CFEPS plutinos now allow us to improve the details of the plutino model to explore other aspects of the resonance that were not accessible with a sample size of eight.

4.1. The Plutino Inclination Distribution

We find that an orbital-inclination probability distribution of the form

$$P(i) \propto \sin i \exp\left(\frac{-i^2}{2\sigma_{32}^2}\right) \quad (4)$$

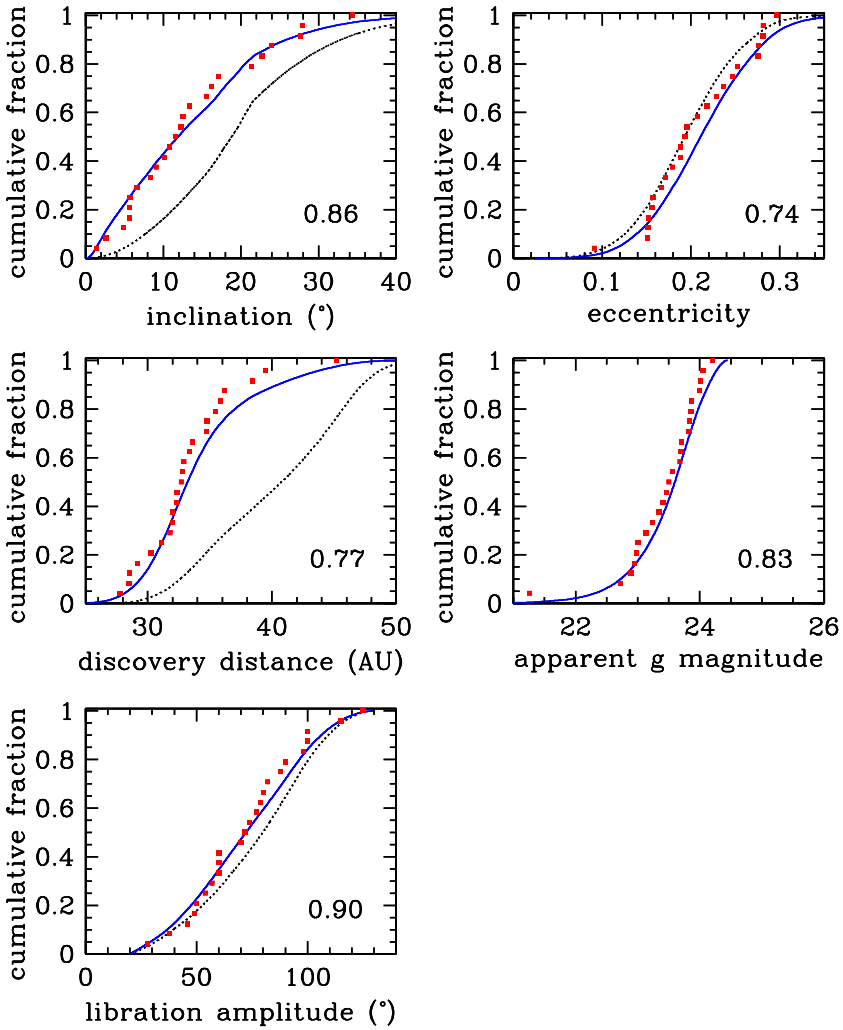

Figure 3. Cumulative distributions of the five variables on which we perform statistical analysis for the plutinos. Red squares show the distribution of the 24 detected CFEPS characterized plutinos. The dashed black line shows the distribution of the intrinsic plutino population from our favored L7 model, and the thicker blue line shows the resulting distribution of that model's simulated detections. The number in each panel is the bootstrapped Anderson–Darling statistic, indicating the percentage of randomly drawn samples from the simulated detection distribution that had worse Anderson–Darling values than the real detections. We reject the model if any parameter has a bootstrapped value <0.05 (meaning only 5% of randomly drawn samples have a worse Anderson–Darling statistic than the real detections).
(A color version of this figure is available in the online journal.)

provides an acceptable representation of the intrinsic plutino inclination, with $\sigma_{32} = 16^\circ$ giving the best match (first panel of Figure 3). The CFEPS 95% confidence intervals for this functional form range from 12° to 24°. The lower end of this range overlaps with the estimates of $\sigma_{32} = 10^{+3}_{-2}$ deg (Brown 2001) and $\sigma_{32} = 11^\circ \pm 2^\circ$ (Gulbis et al. 2010), which use a heavily overlapping sample. As was the case in Kavelaars et al. (2009), the CFEPS survey continues to favor a significantly hotter inclination distribution for the plutinos, with 4 of our 24 plutinos having $i > 23^\circ$, whereas none of the 51 DES plutinos have $i > 23^\circ$. We do not believe this is a sample-size problem, but rather an issue of preferential loss of the large-inclination detections in surveys that did not systematically acquire tracking observations 2–4 months after discovery in the initial opposition; Jones et al. (2010) illustrate how this bias enters Kuiper Belt surveys, regardless of the orbit-fitting method used for the short-arc orbits. Since plutinos are often discovered at nearby 30–35 AU distances, their faster rate of motion makes accurate determination of their orbits more critical than classical objects, and they are easier to lose at the next opposition.

Our plutino inclination distribution is quite similar to the inclination distribution of the "hot" component of the classical Kuiper Belt, making it plausible that the plutinos and the hot classical belt are both captured populations whose inclination distribution neither affected their capture probability, nor was i critical for post-capture erosion over the solar system's age. We have shown that trying to use the same bimodal inclination for the plutinos as for the classical belt yields rejection at far more than 99% confidence.

We also explored a functional form of $P_2(i) \propto \sin^2 i \ \exp((-i^2)/(2{\sigma_s}^2))$ for the plutinos, which is roughly a Maxwellian distribution for the velocity component perpendicular to the plane. This functional form also gives perfectly acceptable matches to the CFEPS detections, with a best match at $\sigma_s = 11^\circ$ and an acceptable range (95% confidence) from $\sigma_s = 8.^\circ5$–$13.^\circ5$. However, because this parameterization did not give a significantly better match, nor did it change the total population estimates by more than their uncertainties, for ease of comparisons with the literature we have elected to retain the $\sin(i)$, rather than the $\sin^2(i)$, formulation.

We checked our plutino sample's colors, tabulated in Petit et al. (2011), for a correlation with inclination or "size" via H_g (Almeida et al. 2009; Murray-Clay & Schlichting 2011), but find no significant correlation. We postulate that the size versus inclination correlation is an artifact of the survey depths that found them (with shallow wide-area surveys finding essentially all $H < 5$ plutinos far from the ecliptic, whereas most fainter plutinos have been found in ecliptic surveys which do not cover enough area to find the few $H < 5$ TNOs near the ecliptic). Our plutino sample does not quite go deep enough (past $H \sim 8.5$) to have enough discrimination to see if the smaller plutinos become bluer; our colors are all uniformly blue.

4.2. The Plutino Kozai Sub-component

Two (8%) of our 24 CFEPS plutinos (L4h07 and L4k01) are also in the Kozai resonance; their Kozai classifications are secure using the Gladman et al. (2008) nomenclature. The argument of pericenter for a Kozai plutino librates around $\omega = 90^\circ$ or 270° due to the fact that the resonance affects the angular precession rate, so although Thomas & Morbidelli (1996) show that the Kozai effect in the non-resonant Kuiper Belt appears only at large e and i, inside the 3:2 resonance the Kozai resonance can appear for even moderate-inclination plutinos (Morbidelli et al. 1995). The libration amplitude A_ω depends on the initial e, i, and ω. The plutinos L4h07 and L4k01 both librate with a period of ~4–5 Myr, both are in the $\omega = 270^\circ$ Kozai island,[12] and have libration amplitudes of $A_\omega = 30^\circ$ and 50°, respectively.

With only two Kozai plutinos, the modeling we have done exceeds the level of detail needed to deal with the detections, but we present our efforts as a guide to the modeling that will be needed once characterized samples grow. We used the fourth-order averaged Hamiltonian given by Wan & Huang (2007) to provide a reasonable approximate dynamics for the Kozai plutinos in the CFEPS Survey Simulator (see the Appendix for details). Kozai-librating plutinos have coupled oscillations of ω and e (and hence i because the product $\cos i \sqrt{1-e^2}$ is constant, proportional to the angular momentum's z-component) that are determined by the value of $\cos i_{\max}$ corresponding to the $e = 0$ trajectory with the same angular momentum. Looking at the full set of Kozai plutinos in the Gladman et al. (2008) compilation, we found that using a set of Kozai trajectories corresponding to the $i_{\max} = 23\overset{\circ}{.}5$ Kozai Hamiltonian with different initial $e_{\min}$ values provided a range of Kozai librations sufficient to model the current sample.

Having this Kozai dynamics model, we proceeded to modify the L3 plutino model by introducing the Kozai fraction f_K parameter, which is the intrinsic fraction of the plutinos that are also librating in the Kozai resonance. By running a one-parameter set of models, we find that an intrinsic Kozai fraction of $f_K = 10\%$ gives the apparent CFEPS fraction of 8%; that is, given the longitude coverage of the CFEPS, there is a mild bias against the detection of Kozai librators. This $f_K = 10\%$ fraction is similar to previous estimates (Chiang & Jordan 2002; Nesvorný et al. 2000). Although not very constraining, our formal 95% confidence upper limit is $f_K < 33\%$ so many more plutinos from characterized surveys will be required to accurately measure f_K.

Tiscareno & Malhotra (2009) point out that because the Kozai plutinos are somewhat more stable than the average plutino, the Kozai fraction should have slowly grown with time. Dynamical simulations that attempt to create the plutino orbital structure must thus "erode" their populations to the modern epoch and then state distributions of libration amplitude for both the 3:2 resonant argument and the Kozai libration amplitude, which may be matched to future debiased surveys. LSST may provide enough resonant-TNO detections (LSST Science Collaborations et al. 2009) to use these distributions as diagnostics.

4.3. The Plutino Size and Eccentricity Distribution

With 24 detections, we can now independently measure the standard H-magnitude distribution slope α in the formulation $N(< H) \propto 10^{\alpha H}$ for the plutinos. This is important because, as Kavelaars et al. (2009) showed, the distribution of plutino detection distances is a sensitive function of the combination of the α, e_c, and e_w parameters (where the latter two are the center and width of a Gaussian e distribution). Detection biases favor finding larger-e plutinos at small distances. This is simply understood; when a small-body population has a steeply increasing power-law size distribution, any flux-limited survey is very strongly biased toward detecting the hordes of smaller objects that come above the flux limit only at perihelion. Because of these considerations, surveys really only measure the slope of the size distribution which correspond to the H-magnitude range for the population in question near perihelion; for CFEPS plutinos this means that we constrain the value of α for the range $H_g = 8$–9; smaller plutinos are undetectable and larger ones are too rare to be statistically constrained.

We proceeded to run a very large grid of models covering the plausible ranges of α, e_c, and e_w, as preliminary explorations clearly showed these parameters were correlated. The results (Figure 4) give confidence regions for our plutino model, where the figure shows cuts in three perpendicular planes through the best-matching model, with $\alpha = 0.9$ for all plutinos, and $e_c = 0.18$ and $e_w = 0.06$ for the non-Kozai component (however, these parameters remain valid even if the Kozai sub-population's dynamics is ignored in the modeling). For these experiments the inclination distribution and libration amplitude are kept fixed (and experiments showed they are only weakly coupled to the α, e_c, and e_w triad). A model is rejected if at least one of the distance, eccentricity, or magnitude distributions of the simulated detections disagree (via an Anderson–Darling statistical test) with the real CFEPS detections. We consider models outside the 5% contour rejected.

As Figure 4 shows, our 24-plutino sample is able to meaningfully constrain the properties of the plutino size and orbital distributions. The cumulative e, detection-distance, and apparent m_g distributions corresponding to our nominal model ($\alpha = 0.90$, $e_c = 0.18$, $e_w = 0.06$) were shown in Figure 3. As can be seen, there is the expected mild bias toward the detection of higher-e plutinos. Much stronger is the remarkable bias seen in the (heliocentric) discovery distance d distribution; 22 of the 24 CFEPS plutinos were detected with $d < a_{3:2} = 39.4$ AU, even though any object on an eccentric orbit spends more than half its time further than its semimajor axis. As Figure 2 shows, CFEPS covered a large range of ecliptic longitudes and is thus extremely sensitive to the plutino distance distribution. It is not surprising that the most distant CFEPS plutino (L5c11) is roughly opposite to Neptune on the sky. However, the preponderance of low-d detections demands steeper slopes for the magnitude distribution and large median eccentricities e_c. The median plutino e in the MPC from the Gladman et al. (2008)

[12] We do not believe there is any statistical significance to both Kozai objects being in the same ω island; the MPC sample has roughly equal numbers in each island. Pluto itself is in the 90° island.

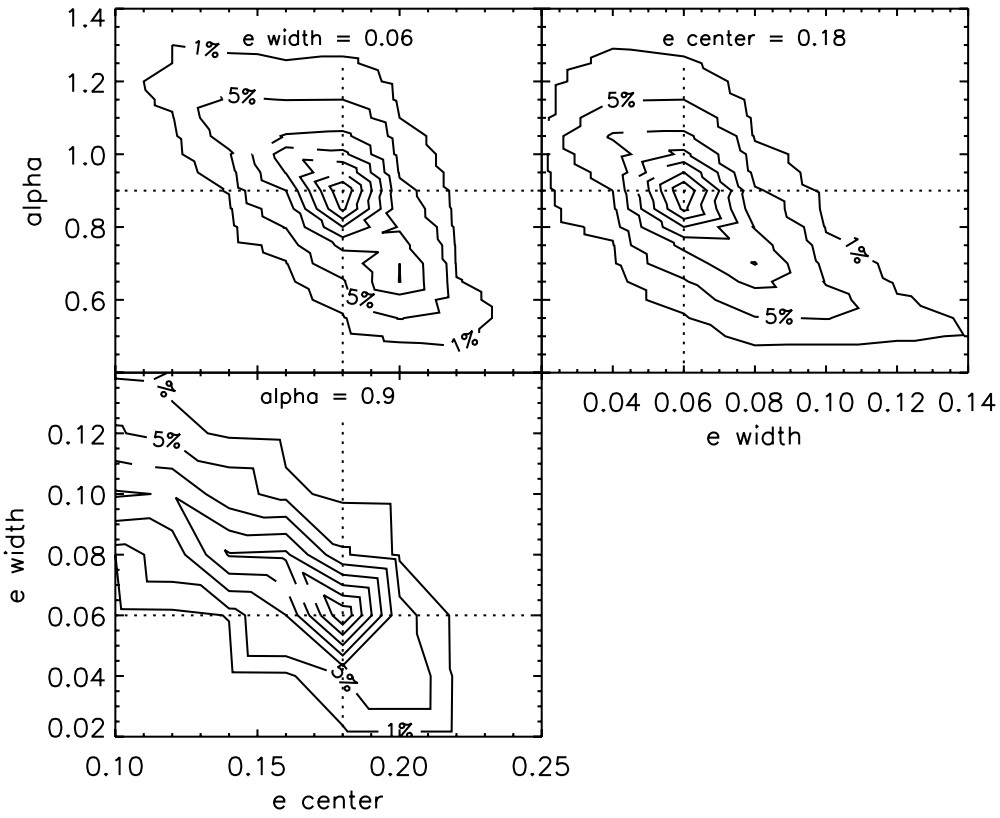

Figure 4. Confidence regions in the plutinos orbital model parameter space. Three perpendicular slices through the (α, e_c, e_w) parameter space, showing the regions interior to which none of the cumulative distributions yield probabilities <5% or <1%. Note the coupling between the parameters; for example, smaller values of e_c are allowed only if the width e_w and the H-magnitude distribution α both rise (or the detection-distance distribution will fail as not being confined enough to small distances).

plutino compilation is 0.224; the hypothesis that the true median intrinsic e is this large or higher is ruled out at >99% confidence.

This analysis demonstrates a correlation between the acceptable values of α, e_c, and e_w. Somewhat shallower H_g distributions (α down to 0.6) are allowed within the 95% confidence range, but such a size distribution requires an e distribution peaked at larger values to maintain the dominance of small-d detections. While α down to 0.6 is not formally rejected by CFEPS, slopes lower than this result in too large a fraction of distant detections. Figure 5 illustrates how going to models beyond the 95% confidence limit alters the d distribution dramatically. Using $\alpha \simeq 0.55$ and the best possible e_c and e_w values still results in a rejectable detection-distance distribution and, unlike our strong suspicion in Kavelaars et al. (2009), we can now formally reject the suggestion in Hahn & Malhotra (2005) that the plutino size distribution is as shallow as $\alpha = 0.54$. On the other end, $\alpha = 1.15$ actually mildly improves the d distribution match, but such a model results in a g-magnitude distribution of the simulated detections being so strongly confined to magnitudes slightly brighter than 24 that this rejects the model at >95% confidence.

The "least rejectable" model we have found has a size index $\alpha = 0.9$, corresponding to a diameter (D) distribution with differential $dN/dD \propto D^{-5.5}$. Again, CFEPS measures this slope only in the $H_g = 8$–9 range which dominates the CFEPS plutino detections. It is interesting to compare this to the $\alpha = 0.8$ estimate from Petit et al. (2011) for the classical main-belt hot population, measured for the $H_g = 7$–8 range (the plutino detections are dominated by physically smaller objects than the more distant main-belt detections). The 0.1 difference between the two estimates is not significant, given the uncertainties. Due to the similarity in inclination and size distributions, our working hypothesis is that the hot population and plutinos (and, as we shall see below, the other resonant populations) share a common origin.

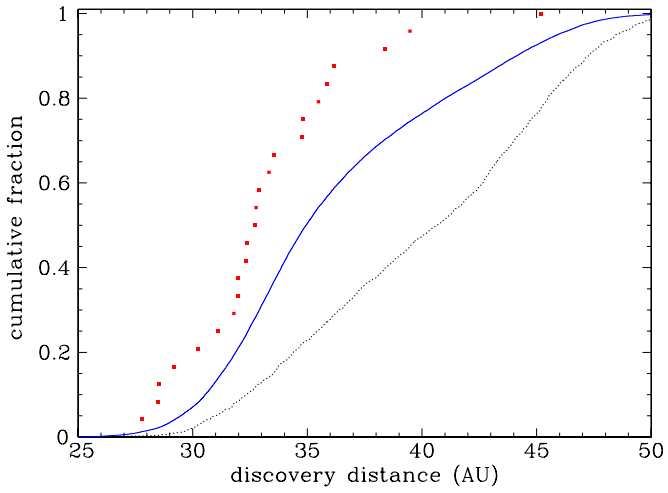

Figure 5. Cumulative plutino distance at detection distribution for a model with size distribution exponent $\alpha = 0.55$. Dotted black line is true heliocentric distance d distribution, which would be detection biased by the CFEPS survey to the solid blue curve; red dots are the CFEPS plutino detections. For such a flat size distribution, too many large TNOs exist at great distance to be detected, which is inconsistent with the concentration to small d present in the CFEPS detections (this model is rejected at more than 99% confidence).

(A color version of this figure is available in the online journal.)

The uncertainty in α makes no significant difference to our plutino population estimate. If $\alpha = 0.8$ (instead of 0.9) our

estimate for the $H_g < 9.16$ plutino population drops only ∼8%, a difference which is much smaller than the current population uncertainties (see below).

4.4. Plutino Libration Amplitudes

Libration amplitudes of the 3:2 resonant argument[13] vary for CFEPS plutinos from $L_{32} = 28°$ (L4j11) to 125° for L4m02. Numerical simulations show that, in the present planetary configuration, plutino libration amplitudes L_{32} larger than about 125°–130° are unstable over the age of the solar system (Nesvorný & Roig 2000; Tiscareno & Malhotra 2009). Any libration amplitudes >130° will be eroded away in the following 4 Gyr of evolution, but most smaller-amplitude librators will be stable. What cosmogonic processes set the distribution of the remaining stable libration amplitudes? Levison & Stern (1995) show libration-amplitude distributions generated in a plutino population captured via gravitational scattering and then damping into the 3:2. Chiang & Jordan (2002) show different libration-amplitude distributions produced by sweep-up capture, depending on Neptune's migration speed.

We first reconfirmed that a uniform L_{32} distribution from 0°–130° was rejected (>98% confidence). This test also showed that CFEPS has a mild bias toward detecting plutinos with $L_{32} < 100°$ due to the longitude coverage. Note that this bias is *not* generic to all TNO surveys; it depends strongly on the longitude coverage and depths of the survey; the L_{32} panel of Figure 3 shows that CFEPS overdetects plutinos in the $L_{32} =$ 50°–100° range relative to their true intrinsic fraction. However, the Survey Simulator allows us to remove this bias. Compared to the L3 plutino model (Kavelaars et al. 2009), we are now able to meaningfully constrain the libration-amplitude distribution. The L3 model used a symmetric triangle probability distribution motivated by the L_{32} compilation in Lykawka & Mukai (2007), that is, a probability that increases linearly from $L_{32} = 0°$ to a peak at 65° and then decreases linearly to $L_{32} = 130°$. The L7 sample shows that this symmetric triangle is now a rejectable representation of the true distribution, producing too many low-libration-amplitude plutinos. We decided to modify the model by changing the low-L_{32} start of the linear distribution and its peak; the linear drop to the end of the probability distribution was retained. An end to the distribution just above the 125° amplitude of L4m02 (which has the largest-known amplitude) is favored by the Survey Simulator analysis of the CFEPS detections. We found that a start of the linear probability distribution at $L_{32} = 20°$ with a peak at 95° provided the best "asymmetric triangle" probability distribution. We tried expanding the range of libration amplitudes to different lower and upper limits while holding the peak of the L_{32} distribution constant at 95°. The lower limits explored were 0° or 20°, and the upper limits were 140°, 150°, 160°, and 170°. While none of these distributions were rejectable at 95% confidence, they provided poorer matches to the CFEPS data than our 20° and 130° nominal model for the lower and upper limits.

Only after arriving at this nominal model did we realize that the resulting asymmetric triangle is very similar to the libration-amplitude distribution shown in Figure 6 of Nesvorný & Roig (2000), which estimates the L_{32} distribution for surviving particles in the main core of the resonance after 4 Gyr of dynamical erosion, based on an assumed initial uniform covering of resonant phase space. We do not think that the debiased CFEPS sample is able to constrain fine details of the current (and thus initial) libration-amplitude distribution, but it is clear that the mechanism which emplaced plutinos must be capable of populating small libration amplitudes efficiently.

[13] Kozai plutinos still have their ϕ_{32} argument librate, with the argument of pericenter librating roughly two orders of magnitude slower than ϕ_{32}.

Table 3
Resonance Populations

Res.	No. of Det.	e_c	e_w	σ_i (°)	Median Pop. ($H_g < 9.16$)	Median Pop. ($H_g < 8$)
3:2	24	0.18_k	0.06_k	$16_{k\,-4}^{+8}$	13000^{+6000}_{-5000}	1200^{+500}_{-400}
5:2	5	0.30	0.10	14^{+20}_{-7}	12000^{+15000}_{-8000}	1100^{+1400}_{-700}
4:3	4	0.12	0.06	8^{+6}_{-3}	800^{+1100}_{-600}	70^{+100}_{-50}
5:3	6	0.16	0.06	11^{+14}_{-5}	5000^{+5200}_{-3000}	450^{+470}_{-280}
7:3	2	0.30	0.06	∼10	4000^{+8000}_{-3000}	320^{+760}_{-270}
5:4	1	0.12	0.06	∼10	160^{+700}_{-140}	10^{+60}_{-9}
7:4	5	0.12	0.06	5^{+9}_{-3}	3000^{+4000}_{-2000}	300^{+400}_{-200}
2:1	5	0.1–0.4	...	$7^{+0.5}_{-5.5}$	3700^{+4400}_{-2400}	340^{+400}_{-220}
3:1	1	0.25–0.55	...	∼10	4000^{+9000}_{-3000}	340^{+800}_{-290}
5:1	1	0.35–0.65	...	∼10	8000^{+34000}_{-7000}	700^{+3000}_{-700}

Notes. Principal parameters for the models of each mean-motion resonance. All resonances used $\alpha = 0.9$ for the H_g-magnitude distribution (that measured for the plutinos). Uncertainties reflect 95% confidence ranges. Population estimates for $H_g < 9.16$ correspond to 100 km diameter (for nominal albedo), while $H_g < 8$ estimates are provided for comparison with the classical-belt population estimates of Petit et al. (2011). The k subscript for the plutinos indicates that these are the parameters for the non-Kozai component.

5. THE POPULATION OF PLUTINOS

Comparison with other resonant populations is discussed in Section 12, but we here put our plutino population estimate in the context of previous literature. CFEPS is sensitive essentially all the way down to $H_g = 9.16$ for plutinos, which corresponds to the frequently used 100 km reference diameter in the literature (for 5% albedo). The CFEPS estimate is

$$N_{\rm plutinos}(H_g < 9.16) = 13{,}000^{+6000}_{-5000}\ (95\%\ \text{confidence}). \quad (5)$$

This can be compared to the factor of two estimate of 1400 from Trujillo et al. (2001), which is the last published measurement independent of CFEPS, and the previous CFEPS L3 (Kavelaars et al. 2009) factor of two estimate of 6000 (scaled to $H_g < 9.16$ utilizing the $\alpha = 0.72$ slope, which now appears to be underestimated). The L3 plutino estimate is consistent with our current estimate, and remains discordant with Trujillo et al. (2001) for the same reasons given in Kavelaars et al. (2009). Table 3 lists both the median $H_g < 9.16$ estimate (which we adopt as standard for all our absolute resonant population estimates, being the limit to which CFEPS had high sensitivity) and an $H_g < 8$ estimate because this value is the CFEPS sensitivity limit in the classical belt, allowing comparison to that population. Due to the different size dependencies now being used, the Kavelaars et al. (2009) $H_g < 10$ estimate should be scaled to the $H_g < 8$ limit by dividing by $10^{2\alpha} = 10^{2(0.72)} \simeq 30$.

Given our current estimate (Petit et al. 2011) of the main classical belt having 130,000 $H_g < 9.16$ TNOs, the plutino population is thus ∼10% of the entire main classical-belt population at the 9.16 limit. Note that the L3 classical-belt estimate was only a restricted portion of the main-belt phase space, and the L7 model now essentially covers the entire non-resonant phase space from 40 to 47 AU. It is important to stress

that the plutino/classical population ratio is H-mag dependent due to the steeper slope of the cold component of the main classical belt. Thus, for $H_g < 8.0$ the plutino/main belt ratio is 15%, in agreement with the estimate of Kavelaars et al. (2009).

6. THE 5:2 RESONANCE

The dynamics of the 5:2 resonance are similar to that of the 3:2 in that low-libration-amplitude TNOs in the 5:2 come to perihelion at a range of longitudes near $\pm 90^\circ$ away from Neptune. The first real 5:2 resonators were recognized by Chiang et al. (2003). As usual, the libration amplitude L_{52} measures oscillations of the resonant angle ($\phi_{52} = 5\lambda - 2\lambda_N - 3\varpi$) around a mean of 180°. Thus, the detection biases are similar to plutinos, making population comparisons likely more robust. Due to their larger semimajor axis near 55.4 AU, 5:2 TNOs spend a large fraction of their orbital period further away than even the most distant plutinos. Although Figure 1 shows that at a given ecliptic longitude low-L_{52} TNOs could be found at several different discrete distances due to their phase behavior, an eccentric orbit still massively biases the detections to be at the perihelia longitudes (constrained by the libration amplitude L_{52} of ϕ_{52}).

The five CFEPS 5:2 objects all have remarkably high eccentricities (in the narrow range 0.38–0.42), inclinations from 2° to 23°, and $L_{52} = 44^\circ$–91°. Because the MPC has 5:2 resonators with $e < 0.38$, we think this concentration for $e \simeq 0.4$ is a statistical fluke; a similar situation occurred with the plutino discovery distances in Kavelaars et al. (2009) which disappeared in the current larger sample. Some 5:2 resonators with well-determined orbits in the MPC sample have eccentricities below $e \sim 0.3$. With only five CFEPS detections we cannot place strong constraints on the internal orbital distribution, so we proceeded to build a model with a similar level of detail as the Kavelaars et al. (2009) plutino model. Luckily, the 5:2 lacks a Kozai sub-component (no known TNO librates in the 5:2, and we are unaware of any theoretical prediction indicating a non-negligible phase space for Kozai inside the 5:2).

The inclination distribution is consistent with being the same as that for the plutinos; Table 3 lists the "least rejectable" value of $\sigma = 14^\circ$, but the large uncertainties mean that identical inclination distributions for 3:2 and 5:2 TNOs is a plausible hypothesis, which we thus adopt. As for the plutinos, we ran a three-dimensional (α, e_c, e_w) grid to set confidence intervals on these parameters. Unsurprisingly, this analysis did not meaningfully constrain α (which allowed the range 0.4–1.2 at 95% confidence, with a broad peak around $\alpha \sim 0.9$). We thus chose to use the plutino-determined value of $\alpha = 0.9$ for the 5:2 and all other H-magnitude distributions for resonant populations for which CFEPS had a detection.

The detected eccentricity distribution for 5:2 resonators is obviously different than that for the plutinos; eccentricities up to $e \simeq 0.4$ exist, corresponding to $q \simeq 30$ AU. The prevalence of orbits with perihelion at Neptune might be taken as firm evidence that this population was emplaced by scattering, but the detection biases also favor low q, so perhaps there are abundant low-e 5:2 resonators that make up only a small fraction of a detectable sample.

We performed a similar grid search for acceptable parameters of an eccentricity distributions with a Gaussian center e_c and width e_w. Figure 6 shows that the most-favored model is indeed a narrow peak centered near $e_c = 0.4$. Like the plutinos, there is a coupling between acceptable values of the distribution's width and center. It is possible that e_c is much lower and the width

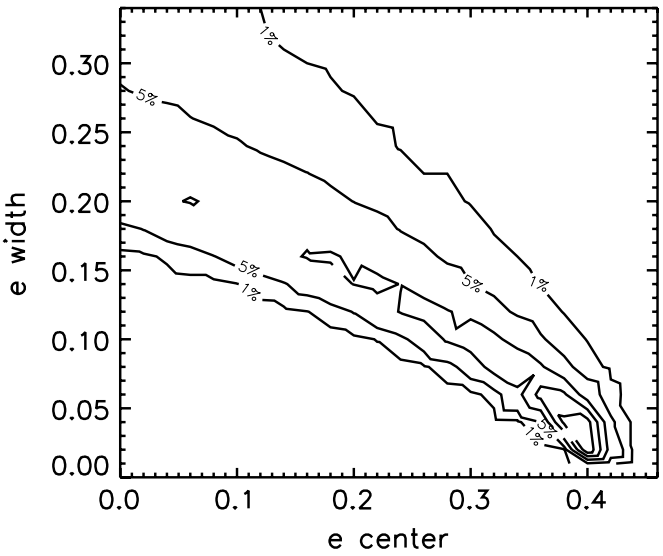

Figure 6. Confidence regions for the 5:2 parameter space, for $\alpha = 0.9$, showing the eccentricity distribution's range of acceptable (e_c, e_w) parameters. Although CFEPS most favors a strongly peaked distribution near $e = 0.4$, a region of lower-e_c centers with larger widths is acceptable inside the 5% limit. Even a Gaussian centered on $e_c = 0$ cannot yet be formally rejected due to the strong detection bias toward larger e.

e_w higher. We find this result to be generic for all the Kuiper Belt resonances; it simply results from extreme bias toward detecting the abundant small TNOs near the perihelia of high-e orbits. Compared to the 3:2, the quality of fit of lower-e_c/higher-e_w pairs is not in as great a contrast with the quality of the most favored case. We thus elected to base our nominal 5:2 model and population estimate (Table 3) on (e_c, e_w) = (0.3,0.1) (along the ridge) instead of the absolute peak where (e_c, e_w) = (0.4,0.04); the latter case has a 40% smaller population but cannot be correct given that two 5:2 resonators (2005 SD_{278} and 84522) exist in the MPC sample with $e < 0.3$. If the real 5:2 population has many even-lower eccentricity orbits, the population will be somewhat larger than our nominal estimate; for example, even the rather extreme case of (e_c, e_w) = (0.14,0.18) yields a population 40% larger than our nominal estimate.

The nominal 5:2 model produces a population estimate of 12,000 5:2 resonators with $H_g < 9.16$ (Table 3). Although the 95% confidence limits range from 4000–27,000, the favored population is, perhaps surprisingly, essentially equal to that of the plutinos. This is an unexpected result, as it indicates that the detection bias against 5:2 is roughly a factor of five stronger, due to the larger values of a and e, both of which result in the population being much less detectable than the plutinos. We will return to the cosmogonic implications of this in Section 12, having compiled population estimates for other resonances.

The ability to capture TNOs into the 5:2 via either sweeping up a pre-existing belt or capturing scattering TNOs into the resonance was discussed by Chiang et al. (2003). These authors showed that although resonance sweeping could capture into the 5:2, the observed orbital element distribution and the apparent 5:2/2:1 detection ratio could only be explained if the resonances captured objects with a pre-excited e and i distribution. Creating most 5:2 TNOs by "resonance sticking" out of a disk of TNOs scattering off Neptune (in the current planetary configuration) was argued to be untenable.

The Levison et al. (2008) scenario of having the resonant populations trapped during a phase of outward migration can

produce lower-e and lower-L_{52} TNOs after Neptune's eccentricity is damped, and in one simulation produced a concentration of $e \sim 0.4$ resonators (although this simulation fails to produce other needed constraints like the inclination distribution). This scenario is promising as a general way to trap resonant populations out of an already-scattering population. In their comparison with 5:2 resonators from the most successful Levison et al. (2008) run (for that resonance) with the MPC sample, the total range of e, i, and L_{52} almost span the values of known MPC TNOs, but their comparison was not corrected for observational biases which favor low-i and high-e detections, which means that the run produces a simulated 5:2 population that has too many large-e and low-i orbits.

The following two sections deal with the n:3 and n:4 resonances. Some readers may wish to skip forward to Section 9's discussion of the n:1 resonances and cosmogonic significance, especially on a first reading.

7. THE n:3 RESONANCES

The n:3 resonances have three different ecliptic longitude centers (Figure 1 shows the examples) at which objects are currently coming to perihelion: one is opposite Neptune and the others are 60° ahead and behind. A resonant-argument libration of amplitude L then results in an angular deviation of $L/3$ on the sky of the perihelion-longitude location relative to these three centers, over the course of a full cycle of the resonant argument.

CFEPS has detections in the 4:3 (4 TNOs), 5:3 (6 TNOs), and 7:3 (2 TNOs). The detection biases for these n:3 resonances are similar in the sense that the CFEPS block locations will not favor one of these three over the other unless they have different libration-amplitude distributions, for which we see no evidence. However, the smaller semimajor axis objects will be favored due to the fraction of time spent in the detection volume.

With a few detections per resonance, we have not attempted to model the internal structure of the resonances, but have made a simple generalization of the n:2 resonances. We keep the same non-symmetric triangle for the libration-amplitude distribution as for the 3:2 (with no amplitudes above 130°). The eccentricity width e_w is also retained, but the central value e_c was moved to correspond to $q \simeq 33$–35 AU. This is consistent with the idea that the resonant objects were largely trapped from a primordial Neptune-coupled population, but is not required by our data. Lower values of e_c are allowed in the same sense as the discussion of the 5:2 resonance; detection biases that lower-e_c/higher-e_w pairs are permissible sufficiently favor the high-e TNOs (which would slightly raise the population estimates). We retained $\alpha = 0.9$ for these resonances.

We did not retain the $\sigma \simeq 16°$ inclination width from the plutinos, as we found all three n:3 resonances favored somewhat lower inclination widths (although the 95% confidence regions allow $\sigma = 16°$). Table 3 lists the favored σ width for each resonance (where the 7:3 is extremely uncertain, so $\sigma = 10°$ was used) along with the population estimates for $H_g < 9.16$ and <8.0. The 4:3 population must be small (<2000 with $H_g < 9.16$, at 95% confidence). Although we have five 5:3 resonators and two 7:3 resonators, the bias against the 7:3 TNOs (which have larger a and e values) results in the true 5:3 and 7:3 being roughly equal (at ~5 times the 4:3 population).

7.1. The 4:3 Resonance

The 4:3 resonance at $a \simeq 36.5$ AU was studied by Nesvorný & Roig (2001), who showed that a resonance amplitude distribution like the 3:2 (of an asymmetric triangle with peak near $L_{43} = 80°$–90°) represented those 4:3 TNOs that survive over the age of the solar system. Although not heavily explored, these authors provide some evidence that the stability of the resonance is not a strong function of inclination; if this is also true for the 5:3 and 7:3 resonances, then confirmation of a colder inclination distribution for TNOs currently in the n:3 resonances would require a cosmogonic explanation (as opposed to being due to later dynamical depletion). Nesvorný & Roig (2001) calculate that, under a simple scenario of excitation of a primordial belt with initial surface density dropping as r^{-2}, the number of 4:3 resonators should be 0.77 that of the 3:2 population, whereas our estimate is 0.06, with 0.77 excluded at more than 95% confidence. We thus confirm that this scenario is excluded, and any Kuiper Belt structure-formation scenario must result in a very weakly populated 4:3 resonance in the present epoch.

7.2. The 5:3 Resonance

The 5:3 resonance at $a \simeq 42.3$ AU has the curious attribute that it is almost precisely at the lower semimajor axis limit of the low-inclination component in the main part of the classical belt. The instability for non-resonant TNOs is due to the ν_8 secular resonance which removes low-i TNOs just interior to $a = 42$ AU. The faster precession caused by the resonant argument for TNOs inside the 5:3 shields its members from the ν_8's effects, so the proximity of the 5:3 and beginning of the low-i classical belt is likely just a coincidence, and not of cosmogonic significance.[14]

Lykawka & Mukai (2007) and Gladman et al. (2008) list 11 TNOs[15] from the MPC as librating in the 5:3. CFEPS detected six 5:3 resonators, two of which were discovered before 2003 (Table 2).

Melita & Brunini (2000) performed a numerical study of 5:3 resonators, showing that the interior of the resonance does not contain a simply connected stable region, and that lower-e orbits appeared more stable in a frequency-map analysis; comparison with real objects was difficult as there was only one 5:3 resonator (1999 JS) at the time; the objects plotted in Figure 3 of Melita & Brunini (2000) with $e < 0.15$ are non-resonant. Lykawka & Mukai (2007) also explored the 5:3 numerically and found that particles surviving the age of the solar system were mostly concentrated in the region $0.09 < e < 0.27$ and $i < 20°$, which is indeed the range occupied by the known 5:3 TNOs.

We note that the 5:3 eccentricities are much higher than the classical objects in surrounding semimajor axes (also obvious for the 7:4). It remains uncertain if this is because these resonant TNOs were captured from a lower-e population and pumped to higher e by migration, or rather if both resonant and non-resonant objects existed with e up to 0.25 and then nearby classical object were eroded away over the age of the solar system. The former scenario seems disfavored when considering distant resonances like the 7:3, which do not appear to have the low-e members they might be expected from a sweep-up scenario into a pre-existing belt (although the selection bias against their detection is strong).

At the other extreme, the *absence* of 5:3 TNOs with $e < 0.10$ might also be seen to argue against "sweep-up" migration (because low-e 5:3 objects could be swept up during the final stages from the classical belt). On the other hand, there is

[14] Some mean-motion resonance can always be found close to any given point in the main Kuiper Belt.

[15] There is a typo in Table 2 of Gladman et al. (2008) in the 5:3 entry for K03UT2S = 2003 US_{292}, whose unpacked designation is mistakenly given as 2003 US_{96}. After 2008, this TNO was numbered 143751.

detection bias against the discovery of the lowest-e members and the Lykawka & Mukai (2007) integrations show that such low-e 5:3 resonators can leak out into the surrounding classical belt.

7.3. The 7:3 Resonance

The 7:3 mean-motion resonance (with $a \simeq 53.0$ AU) is little discussed in the literature due to being beyond the 2:1 resonance and being fourth order (and thus nominally weaker). Lykawka & Mukai (2007) and Gladman et al. (2008) each list three TNOs in the 7:3 resonance; only two of the TNOs were shared (2002 $GX_{32} = 95625$ and CFEPS L3y07 = 131696) at the time, but due to improved orbital information both 2004 DJ_{71} and 1999 CV_{118}, and perhaps $1999HW_{11}$, are also likely 7:3 resonators. Additionally, the CFEPS object L5c19PD is a re-discovery of the lost object 2002 CZ_{248}, whose orbit based on a 1 month arc was given to be $a \simeq 56.6$ AU and the ephemeris was about 0.°5 degrees away from the prediction by the time of our 2005 discovery; CFEPS tracked the object a year before being able to establish the linkage to the short arc from three years earlier.

With only two CFEPS detections, we are unable to strongly constrain the parameters that govern the internal orbital distribution. We find (Table 3) that a model with inclination width like the other n:3 resonances of $\sigma = 10^\circ$ and eccentricity width $e_w = 0.6$ works acceptably as long as the e distribution is centered on $e_c = 0.30$ so that perihelia in the $q = 30$–35 AU range are allowed. As before, lower e_c coupled to larger e_w cannot be excluded. This yields population estimate of 4000 7:3 resonators to factor of three accuracy at 95% confidence, about a factor of three below the 3:2 and 5:2 populations.

8. THE n:4 RESONANCES

The 5:4 and 7:4 resonances are little discussed in the literature, despite them both being populated. The Gladman et al. (2008) compilation lists nineteen 7:4 librators and three 5:4 resonators. The resonant argument forces pericenters to be in bands centered on $\pm 45^\circ$ and $\pm 135^\circ$ away from Neptune. Due to the proximity of these locations to the galactic plane, observational surveys have probably not covered these regions as well as they cover the pericenter longitudes of the n:2 resonances.

8.1. The 5:4 Resonance

CFEPS has only one 5:4 resonator and the DES survey (Elliot et al. 2005) a second, bringing the current total to five known objects. With $a \simeq 35$ AU, the 5:4 is the closest (in semimajor axis) exterior mean-motion resonance to Neptune that is known to be populated, but the proximity to Neptune makes the stable phase space restricted. Malhotra (1996) showed how the zone of stable libration amplitudes shrinks rapidly with increasing e; all known 5:4 librators have e in the range 0.07–0.1. With one CFEPS detection we provide an estimated population of $N(H_g < 9.16) \sim 160$, with factor of five 95% confidence limits. Despite its relative uncertainty, it is clear that the 5:4 population is at least an order of magnitude less populated than the 3:2 or 5:2.

8.2. The 7:4 Resonance

The dynamics of the 7:4 resonance at $a \simeq 43.7$ AU were discussed by Lykawka & Mukai (2005), who showed that the maximum stable amplitudes drops as eccentricities rise. These authors noted that the most dynamically stable part of the resonance ($e = 0.25$–0.30 with $i = 0^\circ$–5°) appears unpopulated, despite it being easier to find TNOs with these eccentricities than the lower eccentricities of the known 7:4 resonators (the largest-e CFEPS 7:4 has $e = 0.21$, while the MPC's orbit for 2003 QX_{91} has $e = 0.25$). Dynamical simulations (Hahn & Malhotra 2005; Levison et al. 2008; Yeh & Chang 2009) rarely show occupation of the $e > 0.25$ region, so the lack of $e > 0.25$ 7:4 TNOs seems in line with model results that this region was not populated during the Kuiper Belt sculpting process.

Examinations of the dynamical "clones" of the nominal classifications show that the phase space of the resonance is extremely complex. Even relatively long-arc orbits show great variation in libration amplitude among the clones, and thus our tabulated libration amplitudes are only accurate to a factor of two. A striking aspect of the CFEPS 7:4 detections is their preferentially small inclinations. When fitting a $\sin(i)$ times a Gaussian distribution, we reach the same conclusion as Gulbis et al. (2010) that the acceptable σ widths are considerably colder than for other Kuiper Belt sub-populations. Our 95% confidence range for the inclination width is 2.°5–14°, with 5° being favored, in good agreement with the Gulbis et al. result. Lykawka & Mukai (2005) had already shown that 7:4 resonators with $i > 10^\circ$ are much less likely to survive the age of the solar system; thus, the colder inclination distribution cannot be taken to be a direct signature of the trapping process, although the preference for $e < 0.25$ may be such a test.

9. THE n:1 RESONANCES

The n:1 resonances require more modeling care because of the presence of symmetric and asymmetric libration islands (see Beauge 1994 and citations to it). That is, instead of the resonant argument oscillating symmetrically around 180°, there are three possible modes. The symmetric mode is centered on 180° but, unlike for the resonances discussed earlier, there is a lower limit for the symmetric libration amplitude because the asymmetric islands occupy the phase space where low-amplitude libration occur. The asymmetric librators have libration centers that depend on the TNO's orbital elements (especially its e) and have an upper bound to their libration amplitudes (Malhotra 1996). Detailed modeling of the n:1 resonances would require much more information than the CFEPS detections are able to provide. We have thus chosen to use orbital models motivated by analytic studies of the resonances, where our adjustable parameters are confined only to the inclination distribution and the fraction f_s of the TNOs that are in the symmetric mode. The population estimates thus have some dependence on the accuracy of the analytic studies. Although some n:1 librators also show evidence of simultaneously being in the Kozai resonance (Lykawka & Mukai 2007), we simply do not have the numbers of detections to warrant modeling this as an additional sub-component; as for the plutinos we expect that the population estimates are only very weakly (<10%) dependent on the presence or absence of the Kozai sub-component.

9.1. The Twotinos

The name "Twotino" has been given to 2:1 resonant librators. Much has been made in the past of the population ratio of plutinos to twotinos, because this may be diagnostic of migration models (e.g., Malhotra 1995; Jewitt et al. 1996; Chiang & Jordan 2002). An important goal for us has thus been to provide an estimate of the twotino population ratio to both the 3:2 and 5:2 resonances (which we discuss in Section 12). In addition,

Chiang & Jordan (2002) showed that Neptune's migration rate could affect the population ratios of one asymmetric island to the other.

The CFEPS sample provides five characterized twotinos (Table 2). Another twotino detected in the survey, U7a08 (Petit et al. 2011), is associated with the symmetric island but U7a08 is excluded from this resonant study because its faintness puts it below the 40% detection efficiency threshold which CFEPS felt it could reliably debias ("U" means uncharacterized). Unfortunately this is the largest-inclination twotino ($i = 7.^\circ 0$) in our sample.

We elected to use a Gaussian inclination width of 9°, which allows the CFEPS Survey Simulator to provide a large fraction of $i < 7^\circ$ detections, while simultaneously allowing the existence of larger-i twotinos known in the MPC sample.[16] We find that the inclination distribution of the twotinos *must* (at >95% confidence) be colder than for the 3:2 and 5:2 resonances. The lack of large-i 2:1 librators in CFEPS is not statistically alarming, especially when one considers that one does not expect the inclination distribution today to be a Gaussian: Nesvorný & Roig (2001) and Tiscareno & Malhotra (2009) show that long-term dynamical stability of the 2:1 is inclination dependent, with inclinations above 15° being more unstable, especially for symmetric librators. Thus, the colder inclination width does not necessarily provide cosmogonic information. We have verified that changing the inclination width by a factor of two generates only a factor of two variation in the population estimate.

Three of the four characterized asymmetric CFEPS twotinos occupy the island with $\langle \phi_{21} \rangle \simeq 290^\circ$ (sometimes called the "trailing" island because the perihelion longitudes are "behind" Neptune's ecliptic longitude) while the fourth occupies the leading asymmetric island. We thus have an apparent (biased) measure of the "leading fraction" $f_L^{\rm biased}$ of 0.25. This is an interesting contrast to Chiang & Jordan (2002) who reported that all of the twotinos from the DES at that time inhabited the leading asymmetric island, and Murray-Clay & Chiang (2005) discuss the apparent leading/trailing ratio of 7/2 at that time, or $f_L^{\rm biased} = 7/9 = 0.78$. It is clear that our trailing preponderance is due to the depth of the CFEPS L4j, L4k, L5i, and L5j blocks (Petit et al. 2011) which are well placed to find trailing twotinos, while the CFEPS coverage of the longitude where leading asymmetric twotinos come to perihelion is sparse (the L3s block was not especially deep). We used the CFEPS Survey Simulator to show that on average one-third of asymmetric twotinos detected by CFEPS would be in the leading island ($f_L^{\rm biased} = 0.33$) due to our block depth and placement relative to the galactic plane, even if the true population was equally distributed ($f_L = 0.5$) between the two islands. We hypothesize that the DES survey simply had had the opposite selection effect. Murray-Clay & Chiang (2005) suggested calibrating the observational selection effects by using the 3:2 ratio, but the galactic plane confusion is not the same for the two resonances; due to Neptune's position, "trailing" plutinos are not as confused by the galactic plane as trailing asymmetric twotinos. Therefore, precise measurement of a population asymmetry demands an absolutely calibrated survey with well-understood detection efficiency differences for the two relevant portions of sky. To illustrate what limits can be set on the true value of f_L using the CFEPS calibration, we asked the question: How large would f_L have to be before 95% of the time CFEPS would find two or more leading detections (and thus rule out this value of f_L)? The CFEPS calibration demands $f_L < 0.85$ at 95% confidence. For a lower bound, $f_L > 0.03$ is required (95% confidence) to allow the existence of at least one leading twotino detection in CFEPS. The 67% confidence range is $0.35 < f_L < 0.64$ but we prefer to use the 95% range of $f_L = 0.03$–0.85 for the fraction of all asymmetric twotinos in the leading island. The $f_L > 0.03$ limit only requires that the trailing/leading ratio be less than 30, to be compared with ratios up to ∼10 found by Murray-Clay & Chiang (2005) in simulations of asymmetric capture during Neptune migration. This weak observational constraint does not yet provide interesting rejection of cosmogonic theories, but a factor of several more twotinos in well-calibrated surveys has the potential to do so.

The symmetric librator K02O12 = 2002 PU_{170} has libration amplitude $L_{21} = 154^\circ \pm 4^\circ$; over a full libration cycle its perihelion longitude can thus be found anywhere on the sky not within ≃25° of Neptune. The excluded CFEPS discovery U7a08 (not characterized due to its faintness) is an alternating "three-timing" 2:1 object, meaning that during numerical evolution forward in time, its resonant argument switches between symmetric and asymmetric modes. This commonly seen behavior (Chiang & Jordan 2002) does not invalidate a parameterization of the 2:1 as having a "symmetric fraction" f_s because it is reasonable to assume that this fraction is maintained in steady state.

With only five characterized 2:1 CFEPS detections, our orbital distribution is based on abundant theoretical understanding of the resonance's dynamics, rather than an empirical model fit to our detections (which will have too many parameters to be constrained by our five detections). Instead, the range of libration centers, amplitudes, and eccentricities (and correlations between them) are provided from analytic understanding and numerical explorations of the resonance (see the Appendix). This model provides a non-rejectable match, leaving as the only remaining adjustable parameter the unknown fraction f_S of symmetric librators that make up the twotino population.

The symmetric libration fraction is poorly measured. A few such objects are known (Lykawka & Mukai 2007), but again because the selection effects are very different for symmetric versus asymmetric librators only a survey with well-characterized sky coverage can provide an estimate. With only one in five characterized detection in CFEPS being symmetric, we can only weakly constrain f_S. Because the fraction of detected twotinos which are symmetric will depend on a survey's longitude coverage, we can only determine it for our own survey; we did this by running a large suite of models to determine the detected fraction of symmetric detections as function of the intrinsic value and find that our 20% apparent fraction implies $f_S \simeq 0.3$, which we adopt. The remaining 70% of the twotinos are equally divided among the two asymmetric islands. Luckily our population estimate is only a weak function of f_S; we determined that even if f_S were increased to 0.75 the total twotino population estimate rises only 25% (again, this result will not be identical for a survey with different sky coverage).

We find a plutino/twotino ratio to be ∼3–4, similar to the ratio estimated by Chiang & Jordan (2002). An important new result from CFEPS is the fact that the twotinos are less numerous than 5:2 librators, which will be discussed in Section 12.

9.2. The 3:1 Resonance

CFEPS detected two TNOs in the 3:1 resonance, one of which (U5j01PD) was below the 40% detection efficiency threshold.

[16] The only secure twotino with $i > 15^\circ$ is 130391 = 2008 JG_{81}, with $i = 23.^\circ 5$, which appears to be a symmetric librator.

With these statistics we are unable to explore details of the TNO distribution inside the resonance's structure; instead we provide a population estimate, which is likely only accurate to order of magnitude. The dynamics allows both symmetric and asymmetric librators; Malhotra (1996) shows the 3:1's structure. Due to lack of constraint, we retain the symmetric fraction $f_S = 0.3$ used for the twotinos. We use an orbital element distribution inside the resonance essentially the same as for the 2:1, except that the model eccentricities extend up to that necessary to reach $q \simeq 30$ AU.

Chiang et al. (2003) and Hahn & Malhotra (2005) demonstrated that 3:1 librators could be produced in an outward migration scenario into an initially warm ($e \sim 0.1$) pre-existing belt. In both simulations the initial disk extends to at least 55 AU from the Sun, although it is not clear where the warm disk must extend to in order to enable 3:1 trapping. Levison et al. (2008) do not provide information on the 3:1 (or more distant) resonances, confining their discussion to $a < 60$ AU.

The 3:1 librator L5j01PD = 2003 LG_7 = 136120 (Table 4 of Petit et al. 2011) was discovered by the DES survey in 2003 (Elliot et al. 2005) and independently re-discovered by CFEPS in 2005. Despite observations in each and every of five sequential oppositions from 2003 to 2007, we are unable to securely determine if the object is a symmetric or asymmetric librator, although the symmetric case is favored. Lykawka & Mukai (2007) classified the object as symmetric using the DES data from 2003 to 2006 inclusive (with amplitude $\approx 160^\circ$ for the best-fit orbit) but we find that asymmetric libration is still allowed for orbits consistent with the astrometry. This serves as another example of the need for abundant high-precision astrometry to determine the details of the resonance dynamics. Because this TNO has flux resulting in a detection efficiency below the 40% limit in the L5j block, we do not use it in our population model.

The characterized TNO L4v08, with similar five-opposition coverage, may also be either a symmetric or asymmetric 3:1 librator, with the former slightly favored. The two-night 2004 discovery of L4v08 was already in the MPC astrometric database with designation 2004 VU_{130}, with an orbit putting it at the $d =$ 49 AU aphelion of an $a = 43.9$ AU classical-belt orbit. Note that L4v08 happens to be the most distant CFEPS resonant TNO at $d = 49.7$ AU; L5j01PD is at $d = 33$ AU. Because the 3:1 population must extend to $d \sim 90$ AU, given their $e = 0.4$–0.5 range, the fact that in both cases $d \ll a$ again illustrates the extreme pericenter detection bias caused by the eccentricities and steep size distribution.

Using a 3:1 model similar to the 2:1 model, our population estimate is 4000 3:1 TNOs with $H_g < 9.16$, with factor of three error bars at 95% confidence. The resulting debiased CFEPS 2:1/3:1 ratio estimate of $\sim$1 is not statistically distinguishable from the $\simeq$3.5 estimate in the 50 Myr migration simulation of Chiang et al. (2003), given our uncertainties at 95% confidence. However, the Chiang et al. simulation does not "erode" the surviving resonant populations (given 50 Myr after migration start) for the age of the solar system, which could change the ratio. Hahn & Malhotra (2005) show (see their Figure 6) that for their model's emplaced populations the 2:1/3:1 ratio does not change much during erosion even if both populations drop mildly over 4 Gyr; however, their 2:1/3:1 ratio is $\sim$10, which is rejectable at >95% confidence. Both models plausibly demonstrate the production of 3:1 TNOs with $e > 0.4$ and i up to 20°.

9.3. The 5:1 Resonance

Our sole 5:1 TNO (L3y02 = 2003 YQ_{179}) was provisionally classified as a detached object by Gladman et al. (2008) but flagged as being insecure and quite possibly resonant in the 5:1 (despite already having a three-opposition orbit in 2008). Further tracking observations by our team have resulted in the now-improved orbit being (insecurely) classified as a resonant 5:1 orbit. The high-order resonances are so "thin" in phase space that we postulate other "detached" TNOs are actually in high-order (meaning $j-k$ is large) mean-motion resonances as well. In this case the largest-a orbit consistent with the astrometry is just outside the resonance; however, we are essentially sure that this object is the first identified 5:1 librator.

We note that the detached object 1999 CF_{119}, discovered by Trujillo et al. (2001), has a semimajor axis $\sim$0.3 AU beyond the 5:1 resonance, and the Gladman et al. (2008) analysis indicates the lowest-a plausible orbits are just barely beyond the resonant semimajor axis. A small systematic error in one opposition of the four-opposition orbit might suffice to remove the nominal orbit from the resonance; we thus suggest additional observations.

With $a = 88.38$ AU, $e = 0.579$, and $i = 20.^\circ1$, the detection biases against TNOs like L3y02 are extreme. We used a 5:1 model similar to the 3:1, with asymmetric and symmetric ($f_S = 0.30$) librators, and an inclination width $\sigma = 10^\circ$. Using the single detection, we estimate 8000 TNOs with $H_g < 9.16$ in the 5:1 resonance, an estimate which is only good to a factor of five given our lack of knowledge of the inclination distribution. In particular, if the inclination distribution is considerably hotter than the $\sigma = 10^\circ$ value we have taken from the 2:1 (which seems likely given that L3y02 has an inclination twice that value), then the population estimate will rise. Even at the nominal i-width, the 95% confidence limits permit this resonance to actually be the most populated of all trans-Neptunian space.

10. THE NEPTUNE TROJANS

The first Neptune Trojan was identified by Chiang et al. (2003), and only $\simeq$7–8 are currently known (Sheppard & Trujillo 2010a; Horner et al. 2012). The CFEPS survey did not discover a single Neptune Trojan.[17] As the survey ran, we were very aware of the possibility of detecting 1:1 resonators, and confirm that this has nothing to do with possible detection biases in the survey. The pericenter longitudes of many of the known resonances overlap with the longitudes where Neptune Trojans would spend their time, and CFEPS found resonant and scattering TNOs at distances even closer than those which Neptune Trojans would approach; maximum eccentricities of the known Trojan sample (Sheppard & Trujillo 2010a) of $e \sim 0.05$ would have Neptune Trojans approach no closer than $q \sim 28.5$ AU (farther than the distance at which we discovered and tracked the Plutino L4m02).

We are not alarmed by the lack of such a detection because the fraction of TNOs that are Neptune Trojans is very small. To quantify this, we built a strawman Trojan model and "observed" it through the CFEPS Survey Simulator. The model Trojans had a within 0.2 AU of 30.2 AU, e uniform from 0 to

[17] Although the MPC currently lists L4k09 = 2004 KV18 as an L5 Trojan (Horner et al. 2012), the eccentricity of 0.184 is larger than numerically determined stability limits (Nesvorný & Dones 2002). However, "near" the L5 cloud, the Gladman et al. (2008) analysis shows the object scatters heavily on timescales <10 Myr and thus Petit et al. (2011) reported L4k09 as a scattering TNO, even if on a very short timescale it may be temporarily near the L5 state. Near-Earth asteroids exhibit similar temporary co-orbital behavior (Morais & Morbidelli 2002).

0.08, with ascending nodes and mean longitudes uniformly distributed. Libration amplitudes L_{11} were chosen between 0° and 40°, with the relative number of objects having each libration amplitude increasing linearly from 0° to 40°. Half of the Trojans were set to be trailing ($\langle\phi_{11}\rangle = 300°$) rather than leading ($\langle\phi_{11}\rangle = 60°$). The resonant argument ϕ_{11} was chosen with sinusoidal time weighting with amplitude $\pm L_{11}$ around $\langle\phi_{11}\rangle$, with ω then calculated to fulfill the resonant condition. Since the literature lacks the information needed to estimate the inclination distribution, we chose a hot population with a similar inclination distribution to the non-Kozai plutinos ($\sigma = 15°$). The H_g-magnitude distribution was fixed with $\alpha = 0.8$, as estimated by Sheppard & Trujillo (2010b).

We used the simulator to determine the Trojan population that would give three or more CFEPS detections (on average); this provides the 95% confidence limit for Poisson statistics. This limit is

$$N_{\rm trojans}(H_g < 9.16) < 300 \ \ (95\% \text{ confidence}), \qquad (6)$$

when stated for the same H_g value as the other resonances we study. Sheppard & Trujillo (2010a) estimate that there are ~400 Neptune Trojans with radii >40 km; assuming a 5% albedo, this corresponds to $H_g \sim 9.6$. Scaling our population upper limit using $\alpha = 0.8$ makes the CFEPS upper limit <600 Trojans with $D > 80$ km (95% confidence), indicating that the non-detection of a Neptune Trojan in CFEPS is not statistically alarming given the 400-Trojan estimate of Sheppard & Trujillo (2010a).

11. CFEPS COMPARISON TO A COSMOGONIC MODEL

The CFEPS project has produced three data products, all of which can be accessed at http://www.cfeps.net. First, there is the database of TNO photometry and astrometry for TNOs (characterized and non-characterized) seen in the survey. The characterized list is intimately linked to the second data product: the Survey Simulator, described below. Third, one can obtain an orbital element distribution (called the L7 synthetic model) which is an empirically determined orbital and H distribution which, when passed through our Survey Simulator, provides a distribution of detections statistically indistinguishable from the CFEPS detections.

The true power of CFEPS is the ability to compare a proposed model (resulting from a cosmogonic simulation) to reality. In order to decide how well a proposed Kuiper Belt orbital distribution matches the CFEPS data, one must not just compare the Kuiper Belt model to the L7 synthetic model. This is because CFEPS (or any survey) will be biased toward or against detections in particular parts of orbital parameter space; a model seemingly different from the L7 synthetic model may be biased when "viewed" through the CFEPS pointing history and flux limits into an acceptable match. Similarly, models which appear to match some aspects of the L7 synthetic model may fail dramatically. The only quantitative way to compare a model to the Kuiper Belt via the CFEPS survey is to pass the model through the L7 Survey Simulator and compare the distribution of simulated to real detections. As an example of this process, we here examine the results of a cosmogonic simulation based on the Nice model of giant planet migration (Levison et al. 2008), in order to compare the simulated plutinos with the CFEPS plutino orbital distribution. We chose this model because the plutino libration amplitudes were made available by the authors; providing such information is the state of the art in Kuiper Belt formation models and should become the norm.

We begin with the plutino orbital elements from the end of Run B of Levison et al. (2008), which are those emplaced during the planet-migration process and then survive 1 Gyr "erosion" process to eliminate TNOs that did not have long-term stability on the timescale of the solar system's age. Because there are only 186 surviving model plutinos, we create new particles with very similar orbital elements by "smearing out" those of the existing particles; values of a, e, and i for each new particle were randomly chosen within ±0.1 AU, 0.02, and 5° of the orbital elements of one of the original Nice model particles. We verified that this does not change the overall shape of the cumulative distributions for these orbital elements. Next, ϕ_{32} is chosen sinusoidally from within the values allowed by the known libration amplitude of the Nice model particle. The ascending node's longitude Ω and mean anomaly $\mathcal{M}$ are chosen randomly, leaving ω to be chosen to satisfy the resonance condition. Lastly, the particle's H_g magnitude is chosen from the same $\alpha = 0.9$ exponential distribution used for CFEPS plutinos. The CFEPS Survey Simulator then evaluates whether or not it was detected.

The process was repeated until 10,000 synthetic detections were generated, creating cumulative detection distributions (Figure 7) from which the probability of drawing the detected CFEPS sample is judged. The detected e's and discovery distances provide statistically acceptable matches to the CFEPS detections. In contrast, the hypotheses that the i or L_{32} libration-amplitude distributions of the CFEPS detections could be drawn from this Nice model simulation both fail at >99.9% confidence. The i distribution of the detections that would come from an intrinsic plutino distribution produced by the Nice model is far too cold, and the L_{32} distribution contains too many large-libration-amplitude objects.

Although this model is rejected, this style of model shows the forefront of what models must now provide in Kuiper Belt science. That is, a cosmogonic model should produce TNO orbital distributions for the entire Kuiper Belt, including resonant libration amplitudes and determination of Kozai resonance occupation. Comparison with the current TNO distribution can only really be performed if the cosmogonic simulation (which often focuses on events in early solar system history) is dynamically eroded for the ~4 Gyr interval to bring it to the present day. The fact that the Levison et al. (2008) simulations were eroded for 1 Gyr instead of 4 Gyr might result in small changes to the libration-amplitude distribution of the survivors, but is unlikely to resolve the major discrepancy given that Nesvorný & Roig (2000) and Tiscareno & Malhotra (2009) show that the distribution only changes appreciably with order-of-magnitude increases of timescale.

We note a large number of non-resonant particles surrounding the 3:2 (and some other resonances) with low e at the end of the Nice model simulations. We presume these TNOs to be generated during the phase where the Neptunian eccentricity is shrinking rapidly, which causes the resonance to narrow and "drop out" formerly resonant particles on either side of the resonance. We call these the "beards" of the resonance in this model. This features should be preserved in the Kuiper Belt if the resonances had abundant low-e particles in the resonances when Neptune's e dropped, but these beards are not obviously present in the real Kuiper Belt distribution. We doubt this is a selection effect, but are unable to present a quantitative analysis with the current CFEPS sample size.

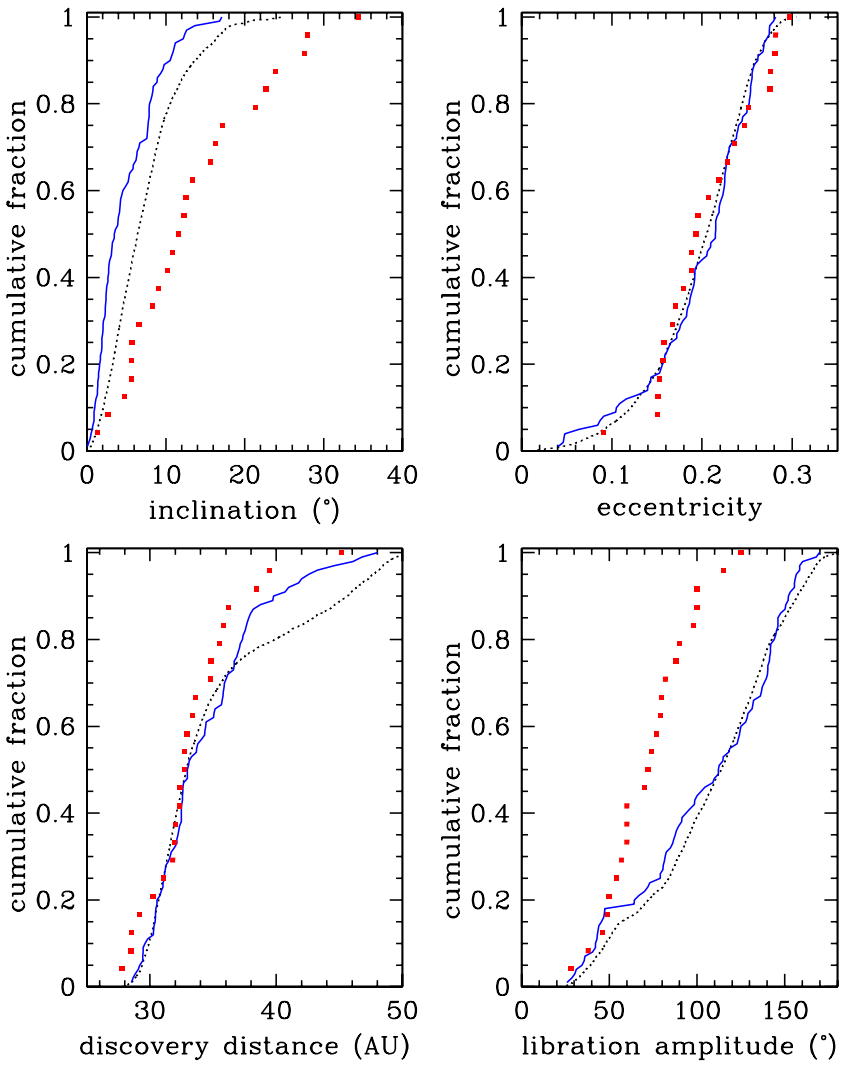

Figure 7. Comparison between CFEPS plutino detections and simulated detections from the Nice model plutino distribution. Red squares are real CFEPS plutino detections, the dotted black line shows the intrinsic Nice model plutino distributions, and the blue line is the simulated detections after running this intrinsic population through the CFEPS Survey Simulator. The magnitude distribution is not shown; this was not provided in the Nice model data but we find using the same H_g-magnitude distribution as for the CFEPS plutinos produced an acceptable match (which is unsurprising given that the e distribution is similar and $\alpha = 0.9$ was chosen to represent the CFEPS detections). While the eccentricity and discovery distance distributions match the CFEPS data reasonably well, the Anderson–Darling analysis indicates the CFEPS i and L_{32} distribution would occur <0.1% of the time.

(A color version of this figure is available in the online journal.)

12. RESONANT POPULATIONS

This work provides for the first time absolute population estimates for a large variety of trans-Neptunian resonances, allowing population comparisons to quantitatively debiased data that takes into account the myriad of observational selection effects. While the ratio of various resonance populations have been identified as potentially diagnostic—for example, Jewitt et al. (1996) already mention using the 2:1/3:2 population ratio to constrain Neptune migrations via models like Malhotra (1995)—the debiasing of the selection effects for the two resonances has never been done to the level of detail presented here. Chiang & Jordan (2002) and Chiang et al. (2003) showed models producing population ratios of resonances to each other (for example, the 5:2 to 2:1) or of sub-islands inside the 2:1 to each other, but again lacked the ability to compare to a survey for which the longitude coverage could be quantitatively debiased for selection effects. Hahn & Malhotra (2005) produced ratios between resonances and to the main belt from a model in the context of an outward Neptune migration into a pre-existing "warm" ($e = 0.1$) belt, while Levison et al. (2008) produced a model in which the Kuiper Belt was moved out to its current location; both of these models were forced to make comparisons to surveys that could account for biases in, at best, an approximate way.

Figure 8 shows the debiasing of the CFEPS, transforming the resonant populations from their biased apparent fractions (left column) to their "true" values (right column, a debiased sample from the models presented in Table 3). An evident result is that the distant resonances make up a much larger fraction of the total resonant population in reality than in the flux-biased sample. Although it is obvious the fraction of large-a resonant TNOs (compared to low-a ones) will be higher in reality than in the flux-biased sample, this effect has never been quantified. In particular, it is obvious that beyond the 2:1 current surveys have just seen the "tip of the iceberg" and the resonant populations contain many more large-i and/or low-e members than either CFEPS or the full MPC sample have yet exposed.

Population comparisons benefit from uncertainty estimates. In particular, the population ratios in the well-studied 3:2, 2:1,

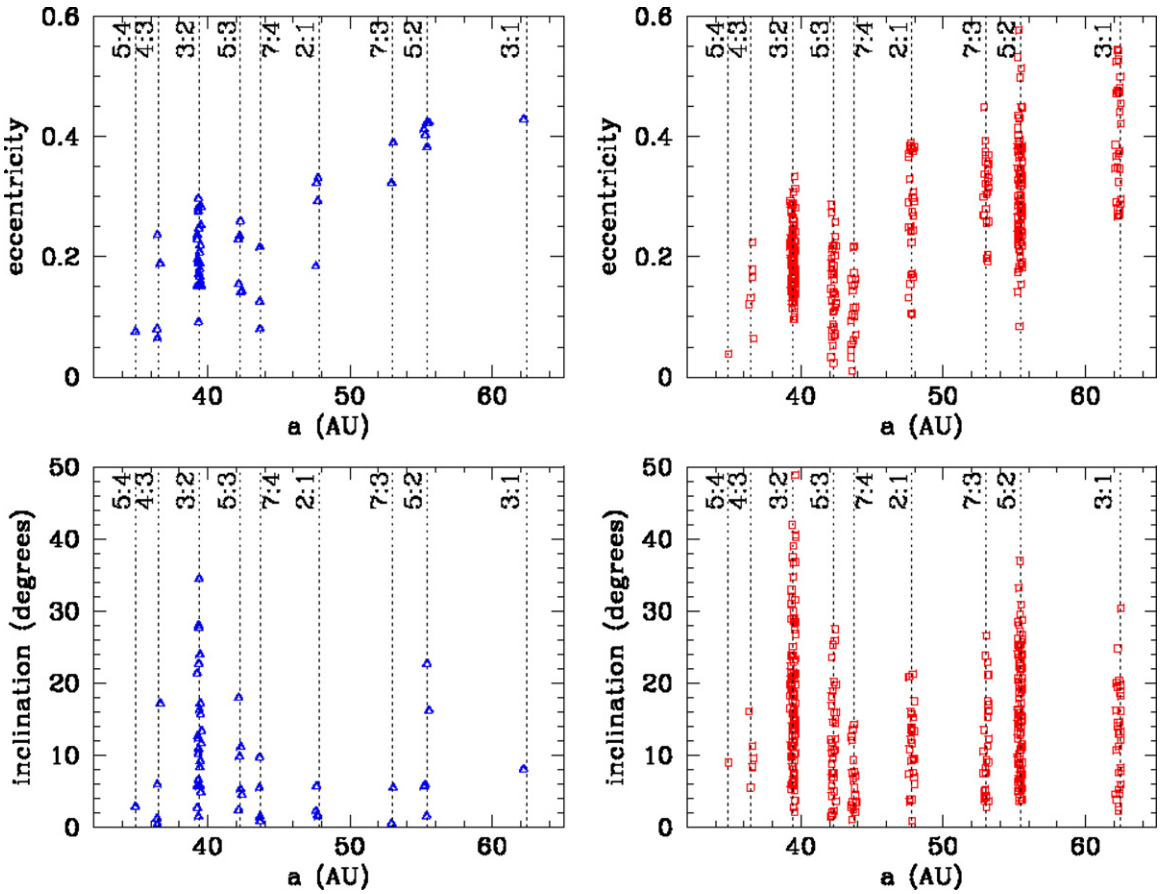

Figure 8. Apparent vs. debiased resonant Kuiper Belt. The two left panels show the (a, e) and (a, i) distribution of the flux-limited CFEPS resonant detections from $a = 30$–65 AU. The right panels show the distribution of their debiased population, scaled so that the plutinos have 100 members. It is obvious that the true Kuiper Belt has a higher fraction of larger-a, lower-e, and larger-i members than the currently detected sample. The absence of low-e resonant TNOs with $a > 46$ AU is not absolutely required by our modeling due to the detection biases against them.

(A color version of this figure is available in the online journal.)

and 5:2 are desirable. To obtain a set of absolute population estimates, we drew particles at random from our model orbital and H-magnitude distributions until obtaining the true number of CFEPS detections for a given resonance (Figure 9). There is an essentially Poisson distribution of plausible "true" populations that will allow the observed number of detections, explaining the shape to the histograms in Figure 9; the median is reported in Table 3 along with the upper and lower limits which leave only 2.5% of the measurements in each tail. Although we use conservative 95% confidence regions (resulting in large stated uncertainties), CFEPS is for the first time able to provide measurements of the resonant populations that take into account the longitude coverage and relative depth of its survey patches.

One of the most striking results (Figure 9) is that the best-estimate populations for the important resonance trio 3:2/2:1/5:2 are in the ratio ∼4/1/4. To our knowledge, this is in stark contrast with all previously published models; those which obtain a weakly populated 2:1 (relative to the 3:2) never simultaneously have a 5:2 population equal to that of the plutinos. The simulations of Chiang et al. (2003) showed a huge 2:1/5:2 ratio unless migration occurred into a hot disk which dropped the ratio to roughly 3/2 (to be compared to the 1/4 ratio we favor), with a plutino population even larger than the 2:1. These authors ruled out "resonance sticking" of scattering TNOs as the dominant production method for 5:2 resonators due to the incorrect libration-amplitude distribution (a conclusion we share based on the small L_{52} amplitudes for the CFEPS detections). Hahn & Malhotra's (2005) simulations into a warm primordial disk exhibit 3:2/2:1/5:2 ratios of about 2/5/1, and Levison et al. (2008) produce 8/3/1. That is, all simulations to date produce fewer 5:2 resonators than twotinos by factors of several, whereas CFEPS indicates that the reverse is true (and rules out the 2:1 being more populated than the 5:2 at >95% confidence). This is thus an important new constraint on formation models.

This kind of constant also holds for more distant resonances. Both the 3:1 and 5:1 have best-estimate populations larger than the 2:1 (although uncertainties are large), indicating that large-a resonant orbits must be efficiently populated by formation models. In models like Levison et al. (2008), where the Kuiper Belt is transplanted out, this is difficult to do because large-a orbits are inefficiently generated. The hypothesis that these objects are instead swept into $a > 50$ AU resonances from warm or hot populations located at these distances before planet migration is faced with the problem of explaining where all the non-resonant TNOs have gone.

This realization that the distant resonances are heavily populated opens the possibility that the current scattering population is dominantly being supplied by abundant resonant escapees. If true then the resonant reservoir would be the ultimate source of Jupiter-family comets (JFCs), through the chain: resonant ⇒ scattering ⇒ Centaur ⇒ JFC. Due to their chaotic boundaries, the resonances provide a "leakier" source of scattering TNOs than the classical belt and most TNOs escaping a

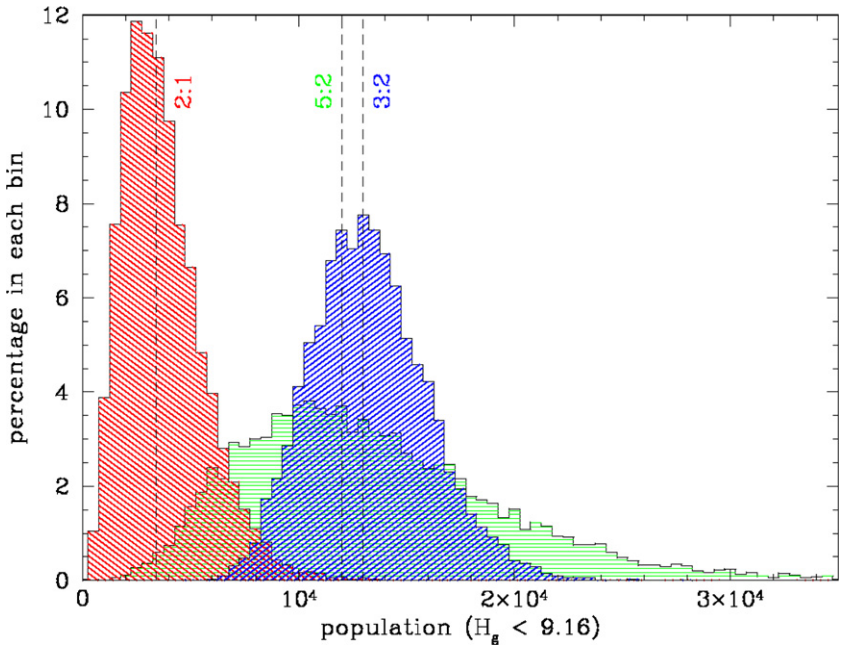

Figure 9. Population estimates for the 3:2, 5:2, and 2:1 resonances. Each histogram is a separately normalized distribution of population estimates which yield the correct number of detections for that resonance. Vertical lines show the median of the population estimates for each resonance. Although the 2:1 and 5:2 histograms overlap, the probability that the 2:1 population is larger than the 5:2 population when both are randomly drawn from these distributions is <5%.

(A color version of this figure is available in the online journal.)

resonance would immediately find themselves on Neptune-coupled orbits and begin scattering.[18] In such a scenario the escape rate from all resonances would balance the loss of actively scattering objects to the Centaur population or ejection from the solar system. The flaw in this scenario is that there seem to be too many scattering TNOs in the current epoch to permit them being anything other than the decaying remnant of a huge primordial population (Duncan & Levison 1997). Petit et al. (2011) estimate (to order of magnitude) that there are currently ~5000 $H_g < 9.16$ actively scattering TNOs (with a clarification on the definition of this population); this is too large a fraction of the sum of the resonant populations in Table 3 to permit the scattering population to be in steady state. Volk & Malhotra (2008) call into question even the "decaying remnant" scenario as the supply rate they estimate from the metastable Kuiper Belt (mostly a mix of detached and resonant objects with $a > 50$ AU and $q > 33$ AU) into the JFCs seems too low given their extrapolation of observational estimates of the "excited" ($i > 5°$) population in the 10–100 km size range. This analysis should be re-done however because Volk and Malhotra assumed that essentially all of today's "excited" TNOs (observed by various surveys) are scattered objects contributing to the Centaur supply chain, while in fact the $a > 50$ AU population has a very non-negligible resonant component (Gladman et al. 2008), and Petit et al. (2011) and this present paper show that the actively scattering population is only a tiny fraction of the other "excited" (resonant + hot classical + detached) populations.

The total resonant population is, however, also comparable to the Petit et al. (2011) estimate for the sum of the outer classical and detached populations (of ~80,000 with $H_g <$ 9.16). This permits serious consideration of the hypothesis that most detached TNO population are resonant objects that were dropped out of resonance while the resonant objects were being emplaced, but must generate roughly equal numbers of resonant and non-resonant objects surviving to the present day.

[18] Horner & Lykawka (2010) suggested that the Neptune Trojans alone could be an important Centaur source, but it seems unlikely that the other (vastly more populated) resonances would not dominate the leakage supply.

13. DISCUSSION

Given the available constraints from the structure and relative populations of various Kuiper Belt components, what can one conclude about the processes that emplaced these components? Based on our debiased understanding from CFEPS, we feel that the following constraints are of chief importance.

1. The resonant populations appear to be consistent with all being emplaced from a source population that lacked a cold component. (The differences between them can be plausibly explained by capture or subsequent erosion processes that are inclination dependent.)
2. The inner classical belt and outer classical belt lack a cold inclination component (Petit et al. 2011), with only the main belt having both hot and cold components.
3. The sum of the resonant populations is ≈75% that of the main belt, for $H_g < 8$.
4. The current "actively scattering" disk is ~5% of the main-belt population, with at least factor of two uncertainty.

Although we do not support it here with detailed simulations, we believe that the following scenario could explain the known structure.

A crucial feature is that the cold population is confined to the $a = 42$–47 AU region of the main belt, with a hotter e distribution for $a > 44.4$ AU. We postulate the cold population could be primordial, with an initial outer edge at this 44.4 AU boundary. The plausible scenario consists of all the other Kuiper Belt populations (hot classical, including the inner and outer belts, detached objects, resonant objects, and the currently scattering objects) being planted into the belt via a mechanism similar to that described by Gomes (2003) and Levison et al. (2008), in

which a massive scattering disk is flung out by the migrating giant planets; resonant trapping of the scattering objects and subsequent dropout litters the hot classical population behind the slowly advancing resonances (which are wide and powerful due to Neptune's temporarily larger e_N). Neptune "jumps" out several AU due to encounters with Uranus and both planets decouple due to damping of their eccentricities. Today's resonant objects are those which were still trapped during the final stages of this process as $e_N \rightarrow 0$. Unlike the Levison et al. (2008) model, we posit: (1) the scattering disk extends to very large a already when Neptune "jumped" out to nearly 30 AU. (2) This scattering disk was very hot; essentially the $\sigma_h \simeq 15^\circ$ width which all the non-cold populations share. How this happens is unknown. (3) The cold population is already in place; it is largely unaffected because the 2:1 resonance jumps to or beyond the 44.4 AU edge. Eccentric Neptune is able to dimly "stir" the a/e distribution of the cold disk, keeping most stirred perihelia $q < 44$ AU, before e_N rapidly decays.

A critical constraint is to prevent TNOs from the cold population appearing in either the 3:2 or 2:1 resonance; this requires that after jumping to near $a = 30$ AU, any remaining small outward Neptune migration cannot allow the resonances to sweep through a cold population, because it would readily trap and preserve them (Hahn & Malhotra 2005). Keeping the 2:1 free of low-i TNOs can be accomplished by having the post-jump value of the resonant semimajor axis beyond the outer edge of the cold disk (say, landing in the 45–46 AU range before finishing outward migration by another AU or so). The situation with the 3:2 is more complex because its lack of a cold component seemingly implies that by the time Neptune jumped, the semimajor axis range between the post-jump $a_{3:2} \sim 37$ AU and today's value must have already been empty of cold objects. Although a primordial inner edge of the cold population is not impossible, the fact that the current $a = 42.4$ AU inner boundary of the cold population is at the border of the ν_8 secular resonance allows a scenario in which this strongly unstable secular resonance swept through the ~37–39 AU region prior to any final small-distance Neptune migration; Holman & Wisdom (1993) show that the ν_8 drives particles to Neptune encounters in only ~30 Myr, which is comparable to the migration timescale for Neptune in Levison et al. (2008). In this scenario, the primordial cold objects with $a < 42.4$ AU join the scattering TNOs, but make up only a tiny fraction of this population as they are "diluted" if any of them are later re-planted into the Kuiper Belt. Unfortunately, the timing (and even migration direction) of the ν_8 is unclear; Nagasawa & Ida (2000) show early and rapid migration of the ν_8 inward as the protoplanet disk's mass eroded, but their calculations did not include the probable outward migration of Neptune.

In our scenario, one has an easy explanation for the differences in colors, size distribution, and binary fraction of the cold main-belt fraction; the cold belt was simply steeper, redder, and either formed more binaries or preserved a greater fraction of them, unlike the implanted components (Parker & Kavelaars 2010). Although there is no direct observational timing constraint, this implantation scenario seems more natural if the disk is scattered very early in the solar system's history, without the ~600 Myr delay proposed in the Nice model (Gomes et al. 2005). In fact, our scenario does not stipulate where the "early" scattering component comes from, although the most plausible source is it being perturbed out from the planetesimal-rich giant-planet region interior to 30 AU. At the time of Neptune's jump, this early scattering population must extend to $a > 50$ AU in order to allow efficient trapping into the well-stocked distant resonances.

The mechanism that causes this early scattering population (which is the source for all hot Kuiper Belt populations) to have the needed inclination width of $\sigma \sim 15^\circ$ is unclear. Perhaps the giant planets somehow vertically heated the planetesimal belt before it was scattered out (although in general scattering will pump a and e at least as fast as i). Gomes (2003) manages to produce large-i implantations from a source disk, although the more recent Levison et al. (2008) study produced a much colder implanted population. Perhaps other now-gone ("rogue") planets caused the initial vertical dispersion, although this too seems inefficient (Gladman & Chan 2006). Very nearby stellar encounters could generate the inclinations by scattering objects (e.g., Kobayashi et al. 2005) but preserving the $\sigma \sim 2^\circ$ cold disk in a ~44 AU ring is a very strong constraint.

The following estimates of sub-populations are intended only to provide a coherent picture to a factor of three or so, with all population estimates for $H_g < 9.16$ (roughly $D > 100$ km). CFEPS estimates (Petit et al. 2011) that today's scattering population is $\sim 10^4$. Assuming this is *not* currently in steady state re-supply from another source, Duncan & Levison (1997) estimate that this would require about ~100 times as many scattering objects ~4 Gyr ago; in a scenario where this disk goes to considerably smaller perihelion distances than the current $q \sim 35$ AU, the initial population would have been at least several times larger and we take 10^7 initial $D > 100$ km scattering bodies. In an $\alpha \simeq 0.8$ size distribution, most of the mass in the small end, and the resulting ~10 $M_\oplus$ of bodies, is comfortably smaller than the mass of the outer planets. We take this primordial scattering population to be the source of the high-i populations. Levison et al. (2008) estimate ~0.5% of such a primordial scattering gets trapped into non-resonant orbits, implying a hot classical population of ~50,000, which is comparable to the 35,000 estimated in Petit et al. (2011) when one realizes that it is only the hot main-belt population that is relevant (the cold population being pre-existing in our scenario). In addition, Levison et al. (2008) report that the plutinos make up about 20% of the non-resonant objects implanted in the main belt, or about 10,000 objects, again reasonably in accordance with the CFEPS estimate of 13,000. This scenario is not supported by simulations here, which would need to show that (1) the cold belt could survive the process, (2) the distant resonances can be efficiently filled, and (3) the Levison et al. (2008) trapping fractions are not strongly affected by the hotter primordial scattering population that is required. In this scenario, gradual migration is a relatively unimportant process for the Kuiper Belt's current structure.

Much of the excitement in Kuiper Belt studies comes from the vigorous interplay over the last two decades between observation and theory, and the steady stream of unexpected discoveries in both domains. Much work remains to be done. While there is evidently considerable room for future surveys to improve upon the CFEPS estimates, this can only be done with well-characterized surveys whose selection effects are rigorously monitored. In turn, the debiased orbital elements distributions will lead to much tighter constraints on models seeking to solve puzzles still present in our understanding of how the outer solar system settled to its current state.

We acknowledge the research support of the National Sciences and Engineering Research Council and the Canadian Foundation for Innovation. We thank the queued service

observing operations team at CFHT for their excellence in obtaining the CFEPS observations. J. Hahn and H. Levison provided output from their cosmogonic models, thus allowing the quantitative comparisons between models and observation that are the future of Kuiper Belt studies. Lastly, we acknowledge the historical debt this subject owes to Brian Marsden, and honor his dedication to orbital computation.

APPENDIX

In order to measure the CFEPS bias to get an estimate of a resonance's true population, we select model objects by randomly drawing from a parameterization of the orbital distribution for the given resonance, and assigning an H_g magnitude from a power-law distribution. Each object is then run through the CFEPS Survey Simulator to decide whether or not it was detectable. This is repeated until a requested number of detections is reached; this number is usually either (1) $\sim 10^4$ to obtain a well-sampled distribution of orbits that would be detected if the model was correct or (2) the number of CFEPS detections to get an estimate of the true absolute population of that resonance. In case (1) the orbital distribution of the simulated detections is then statistically compared to that of the real detections to decide whether or not that model is reasonable.

The orbital elements for each object are chosen in a different order depending on which resonance the object is a member of. This is because of the differing internal constraints of each resonance. The plutinos have many detections, allowing a much more in-depth exploration of the possible orbital parameter distributions, as well as having a significant Kozai fraction (Section A.2). The n:1 resonances have symmetric and asymmetric libration islands which must be populated (Section A.3). Other remaining resonances have fewer detections, and thus the model need not be as complex and the orbital element distribution cannot be constrained as well. These selection processes are described below, in order of increasing complexity.

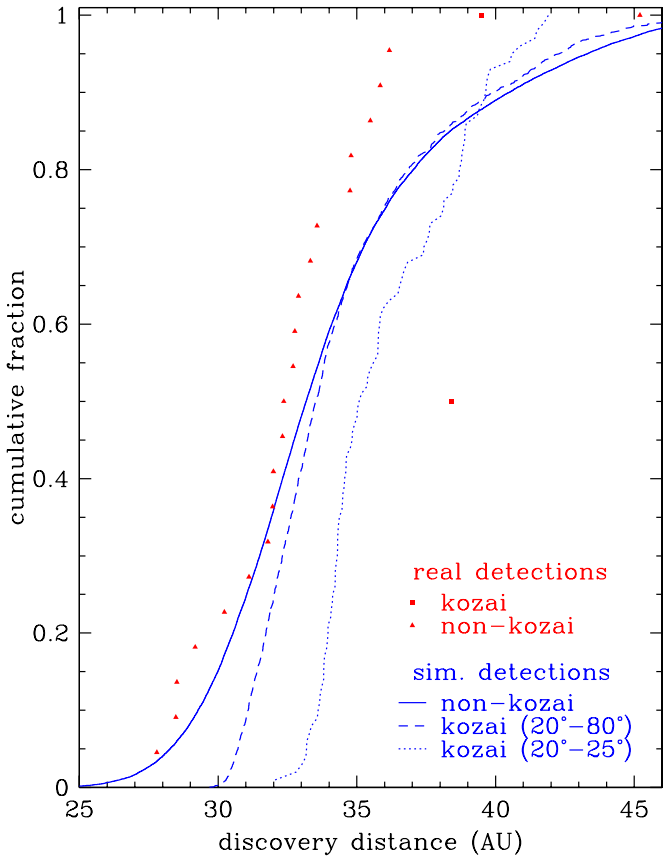

Figure 10. Model predictions for the detection-distance distribution for non-Kozai plutinos, Kozai plutinos with ω libration amplitudes in the range 20°–80°, and Kozai plutinos with libration amplitudes restricted to the range 20°–25°. The cumulative distribution of the real CFEPS detections is also shown. Kozai plutinos, especially those with small libration amplitudes, are preferentially detected at larger distances.

(A color version of this figure is available in the online journal.)

A.1. Simulating the 5:2, n:3, and n:4 Populations

Each of these resonances has between one and six CFEPS detections (Tables 1 and 2), allowing population estimates but no detailed modeling of orbital element distributions. The orbital elements and magnitudes of the synthetic objects in each of these resonances are chosen in the following order.

First, the eccentricity is chosen randomly from a Gaussian distribution centered on the input parameter e_c with a width e_w. Negative eccentricities and those that cause the object to approach the orbit of Uranus ($q \sim 22$ AU) are redrawn. The semimajor axis is then chosen. This is drawn randomly within 0.2 AU of the resonance center. Although in reality the resonances have semimajor axes boundaries that are e dependent, the effect on observability is so weak that given the numbers of detections and the fact that the e distribution is strongly peaked, this makes no difference to our current estimates.

The inclination is chosen independently of a and e. We use the i-distribution parameterization where the probability of a given i is $\propto \sin i \; e^{-i^2/2\sigma^2}$ as proposed by Brown (2001). The ascending node Ω and mean anomaly $\mathcal{M}$ are chosen randomly from 0° to 360°.

The libration amplitude L for each TNO is chosen from a tent-shaped distribution based on the plutino libration-amplitude

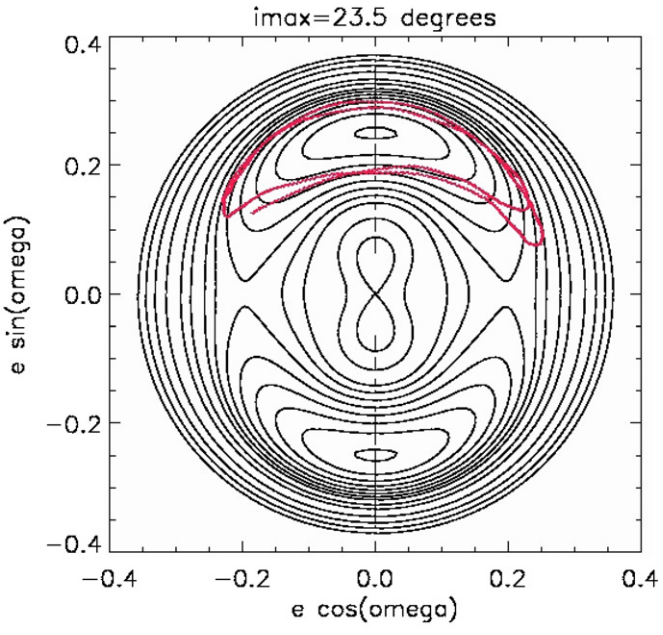

Figure 11. Hamiltonian phase space for the set of Kozai librators used in the CFEPS-L7 plutino model. Here, eccentricity e is the radial coordinate and the polar angle is ω. This diagram's set of contours corresponds to the angular momentum where the zero-eccentricity orbit has $i_{\max} = 23.^{\circ}5$. Also shown (overlain) is the trajectory of a 10 Myr integration of a real Kozai plutino (numbered TNO 69986).

(A color version of this figure is available in the online journal.)

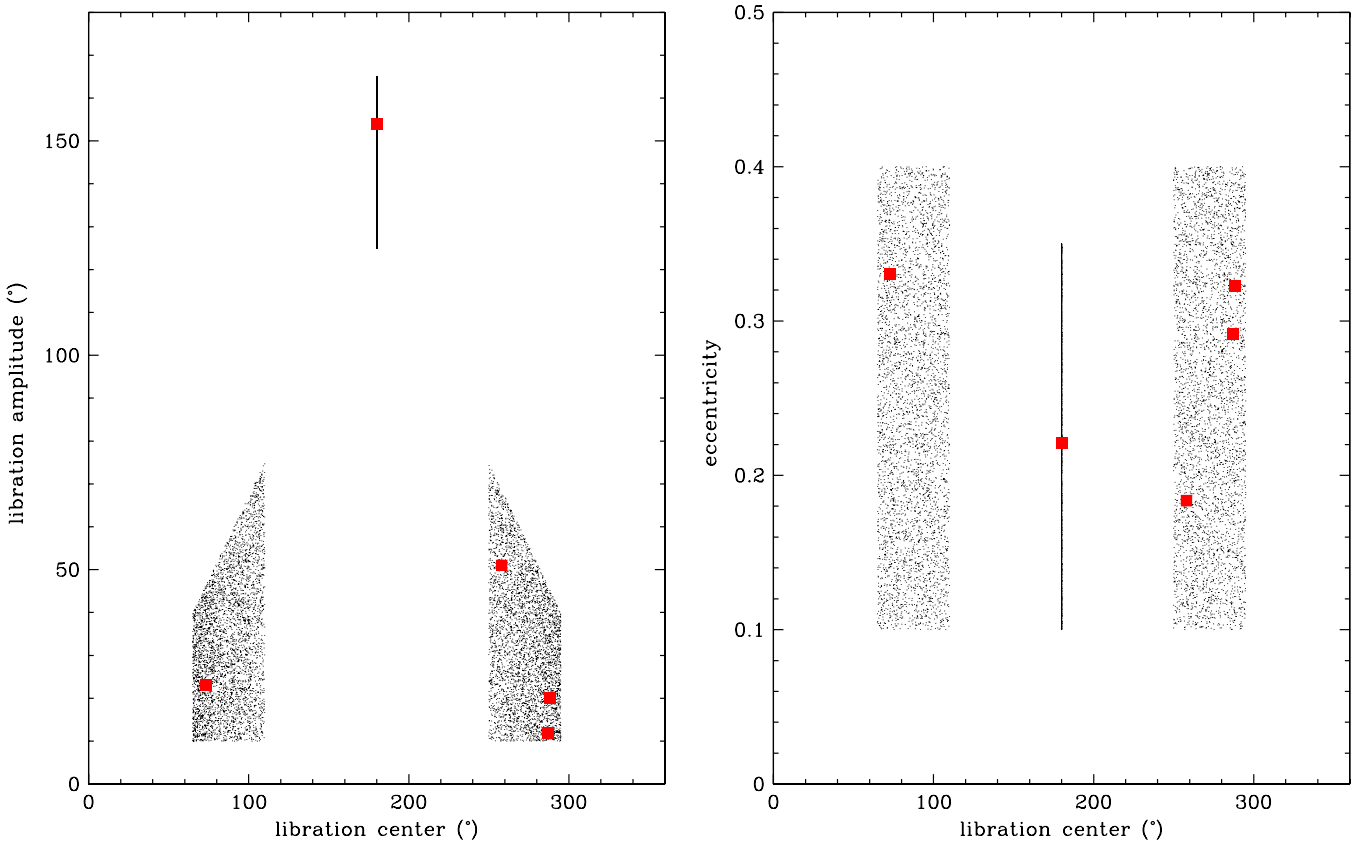

Figure 12. Range of libration amplitudes, libration centers, and eccentricities chosen in our model for the symmetric and asymmetric islands in the 2:1 resonances. The 3:1 and 5:1 models are the same except for a differing range in eccentricities (see the text). Real 2:1 detections are shown as red squares.
(A color version of this figure is available in the online journal.)

distribution suggested by Lykawka & Mukai (2007). However, our study of the plutinos leads us to use a slightly asymmetric shape (see Section 4.4). Our smallest-libration-amplitude TNOs have $L = 20°$, the largest have $L = 130°$, and we put a peak in the libration-amplitude distribution at 95° (that is, the probability increases linearly from 20° to 95° and then drops linearly to zero probability at $L = 130°$).

After a libration amplitude is chosen, ϕ_{jk} is chosen sinusoidally within the range allowed by the libration amplitude (that is, $\phi_{jk} = L \sin \psi$, where ψ is a random phase). The argument of pericenter ω is calculated via $\phi_{jk} = j\lambda - k\lambda_N - (j-k)\varpi$. Finally, the H_g magnitude is chosen from a power-law distribution $10^{\alpha H}$ with a maximum H_g of 11; because this is well below the CFEPS detection limit, our estimate has no dependence on the cutoff.

As each object is generated, its orbital elements and H_g are passed to the CFEPS Survey Simulator, which evaluates its detectability. If it falls within one of the CFEPS pointings and is bright enough, it becomes a synthetic detection. These detections include a certain fraction of objects that will be "lost" due to tracking losses in a magnitude-dependent way (see Petit et al. 2011).

After the desired number of synthetic detections have been acquired, the distribution of synthetic detections and real detections are compared in five parameters: inclination, eccentricity, distance at detection, apparent g magnitude, and libration amplitude (see Figure 3), as discussed in Kavelaars et al. (2009). The Anderson–Darling statistic of the CFEPS detections relative to the simulated detections are calculated for each distribution and the probability of a departure as large or larger than the detected sample is determined by bootstrapping each sample. We consider a model rejectable when at least one of the five distributions has a bootstrapped probability of <0.05.

For these resonances there are insufficient detections to constrain the orbital distribution directly, but this does not result in an important uncertainty in the population estimate. For example, modeling the 5:2 libration-amplitude distribution as flat from 0° to 130° does not result in a rejectable model, like it did for the plutinos, but the $H_g < 9.16$ population only drops to 11,000 from 12,000 (Table 3), a change vastly smaller than the uncertainties, thus showing that our 5:2 population estimate is insensitive to the unknown libration-amplitude distribution. As a second example, changing the e_w value for the 4:3 resonance from 0.06 to 0.10 (allowing easier-to-detect higher-e resonators to exist) drops the $H_g < 9.16$ best estimate from 800^{+1100}_{-600} to 640. We thus believe our Poisson uncertainties due to small numbers of detections dwarf the systematic errors for resonances other than the 3:2.

A.2. Simulating the Plutino Population

The model for TNOs in the 3:2 resonance is identical to the previous section, except that for this resonance we also force a fraction f_K of the objects to simultaneously be in the Kozai resonance. The presence of the Kozai resonance inside the 3:2 is well studied (Morbidelli et al. 1995; Nesvorný & Roig 2000; Wan & Huang 2007). While the Kozai resonance appears only at very large inclinations and eccentricities for TNOs outside mean-motion resonances (Thomas & Morbidelli 1996), inside the 3:2 mean-motion resonance the precession

rates rise sufficiently that at moderate eccentricity ($e \sim 0.25$) and inclination ($i \simeq 10°$–$25°$) the Kozai effect causes libration of the TNO's argument of perihelion around $\omega = 90°$ or $270°$, which results in its perihelion direction being barred from the plane of the solar system.

Two of the 24 CFEPS-detected plutinos are in the Kozai resonance, and the plutinos were already known to include a significant Kozai component (Lykawka & Mukai 2007). The fraction of Kozai librators in the sample is one of our model input parameters. One effect on the detection of plutinos in an ecliptic survey like CFEPS is that Kozai librators are preferentially detected at larger distances than non-Kozais (Figure 10).

During model construction, each object is labeled as either a Kozai or non-Kozai resonator using the model's value of f_K, with the goal being that the simulated detected fraction is satisfactorily in agreement with the true detection fraction of 2/24. If the object is not in Kozai resonance, the orbital parameters are chosen as described in Section A.1 above, with a slight change to the way the semimajor axes are chosen. Instead of just choosing them randomly within 0.2 AU of the center of the resonance, following Figure 7 of Tiscareno & Malhotra (2009), we narrow the resonance's a width linearly to zero as e drops from 0.16 to 0.01; if the drawn (a, e) pair falls outside this bound, a new a and e are drawn.

For the fraction f_K of the plutinos chosen to be Kozai resonators, the following procedure for choosing orbital elements is followed.

First, a Hamiltonian level surface was generated, based on the calculations of Wan & Huang (2007). The libration trajectories in (e, ω) space are determined by the value of the z-component of the angular momentum, which is equivalently labeled by value of $\cos i_{\max}$ for the circular orbit of the same angular momentum. For our current purposes, we picked the single value of $i_{\max} = 23\overset{\circ}{.}5$ based on visual comparison with integrations of known plutino Kozai librators (Figure 11). With this fixed, a libration trajectory is picked at random, corresponding to Kozai libration amplitudes between 20° and 80°. ω is picked sinusoidally between 90° and the maximum ω allowed by the chosen contour. The eccentricity is then found numerically using ω, the chosen Hamiltonian trajectory, and Equation (9) from Wan & Huang (2007). Then i is calculated using conservation of the z-component of angular momentum ($L_z \propto \cos i \sqrt{1 - e^2}$). We then move half the Kozai librators to be around the $\langle\omega\rangle = 270°$ island by the transformation $\omega \longrightarrow 360° - \omega$.

Next, the semimajor axis is chosen in the same manner as for the non-Kozai plutinos, and $\mathcal{M}$ is chosen randomly. Libration amplitudes for ϕ_{32} are chosen in the same way as for the non-Kozais, again using the tent-shaped distribution. ϕ_{32} itself is chosen sinusoidally within the values allowed by the chosen libration amplitude, which this allows the ascending node Ω to be calculated again using the relation $\phi_{32} = 3\lambda - 2\lambda_N - \varpi$.

All the orbital elements have at this point been chosen, so after choosing an H_g magnitude from the same power-law distribution, the object is completely defined and is sent to the Survey Simulator to evaluate whether or not it will be counted as a synthetic detection.

A.3. Simulating the n:1 Populations

Because the n:1 resonances possess several libration islands, the intrinsic orbital distribution must be picked in a more complex way before it is passed into the Survey Simulator. Compared to the plutinos and 5:2, we have far fewer CFEPS objects in these resonances than are needed to directly constrain their complex internal structure. Thus, our primary goal is to obtain a calibrated absolute population estimate based on the expected internal structure predicted by analytic studies of these resonances.

Because the effect on observability of the a-width of the resonance is tiny, we pick the semimajor axis for model n:1 resonant TNOs randomly within 0.2 AU of the resonance center. The eccentricity distribution is more complex because it is linked to the structure of the asymmetric islands. We have incorporated the main features of the resonance from studies of the structure and erosion (see, for example, Chiang & Jordan 2002 and Tiscareno & Malhotra 2009). We define the symmetric fraction $f_s = 30\%$ for each n:1 resonance to be the fraction which is librating in the symmetric island, and as a working hypothesis take the remaining objects to be evenly divided between the two asymmetric libration islands. Symmetric librators have a resonant argument $\phi_{n1} = n\lambda - \lambda_N - (n-1)\varpi$ which librates around $\langle\phi_{n1}\rangle = 180°$ with amplitudes L_{n1} ranging from 125° to 165° (Figure 12), while the asymmetric librators have a more complex distribution. "Leading librators" (to use the terminology of Chiang and Jordan, denoting orbits whose pericenter directions are somewhat ahead of Neptune) are randomly given libration centers $\langle\phi_{n1}\rangle$ in the interval 65°–110°, with libration amplitudes L_{n1} from 10° to 75°, where we redraw if L_{n1} is greater than a limit which linearly rises from $L_{n1} = 40°$ for $\langle\phi_{n1}\rangle = 65°$ to $L_{n1} = 75°$ for objects with 110° libration centers (Figure 12). This range sufficiently reproduces the main characteristics of analytic studies of the asymmetric islands (Beauge 1994), of numerical results on the post-migration distribution (Chiang & Jordan 2002), and of the known 2:1 detections. Half of the asymmetric librators then have their centers moved to the "trailing island" via $\langle\phi_{n1}\rangle \longrightarrow 360° - \langle\phi_{n1}\rangle$. Eccentricities for 2:1 resonators are drawn uniformly in the range 0.10–0.35 for symmetric librators or 0.10–0.40 for asymmetric librators (Chiang & Jordan 2002). For the 3:1 the symmetric/asymmetric e range is 0.25–0.50/0.25–0.55, and for the 5:1 they are 0.35–0.60/0.35–0.65. The dependence of the population estimates on the e range chosen is small; if the 2:1 eccentricity distribution is changed to be uniform from 0 to 0.35 for all three islands, the model's rejectability is not altered (Anderson–Darling e match changes negligibly from 0.69 to 0.47) and the population rises from 3700 (+4400,−2400) to 5700 due to the greater preponderance of harder-to-detect low-e 2:1 resonators in this alternate model. While this test is somewhat artificial because such low-e twotinos are not abundantly present in Chiang & Jordan (2002) or Tiscareno & Malhotra (2009), even this large systematic change only alters the population estimate by half of our estimated uncertainty range.

Inclinations are chosen from a $\sin(i)$ times a Gaussian distribution (as for non-Kozai plutinos and for the other resonances). $\mathcal{M}$ and Ω are chosen randomly from 0° to 360°. ϕ_{n1} is chosen sinusoidally from within the range of possible libration amplitudes around the libration center. Then ω is calculated using the relation $\phi_{n1} = 2\mathcal{M} + \Omega + \omega - \lambda_N$.

Finally, the n:1 object is assigned an H_g magnitude in the same manner as for the other resonances, regardless of which libration island it is assigned to. It is then sent to the Survey Simulator.

REFERENCES

Almeida, A. J. C., Peixinho, N., & Correia, A. C. M. 2009, A&A, 508, 1021
Beauge, C. 1994, Celest. Mech. Dyn. Astron., 60, 225
Brown, M. E. 2001, AJ, 121, 2804
Chiang, E. I., & Jordan, A. B. 2002, AJ, 124, 3430

Chiang, E. I., Jordan, A. B., Millis, R. L., et al. 2003, AJ, 126, 430
Cohen, C. J., & Hubbard, E. C. 1965, AJ, 70, 10
Davies, J. K., McFarland, J., Bailey, M. E., Marsden, B. G., & Ip, W. 2008, in The Solar System Beyond Neptune, ed. M. Barucci et al. (Tucson, AZ: Univ. Arizona Press), 11
Duncan, M. J., & Levison, H. F. 1997, Science, 276, 1670
Elliot, J. L., Kern, S. D., Clancy, K. B., et al. 2005, AJ, 129, 1117
Gladman, B., & Chan, C. 2006, ApJ, 643, L135
Gladman, B., & Kavelaars, J. 2009, Phys. Can., 64, 209
Gladman, B., Marsden, B. G., & Vanlaerhoven, C. 2008, in The Solar System Beyond Neptune, ed. M. Barucci et al. (Tucson, AZ: Univ. Arizona Press), 43
Gomes, R., Levison, H. F., Tsiganis, K., & Morbidelli, A. 2005, Nature, 435, 466
Gomes, R. S. 2003, Icarus, 161, 404
Gulbis, A., Elliot, J., Adams, E., et al. 2010, AJ, 140, 350
Hahn, J. M., & Malhotra, R. 2005, AJ, 130, 2392
Holman, M. J., & Wisdom, J. 1993, AJ, 105, 1987
Horner, J., & Lykawka, P. S. 2010, MNRAS, 402, 13
Horner, J., Lykawka, P. S., Bannister, M. T., & Francis, P. 2012, MNRAS, 422, 2145
Jewitt, D., Luu, J., & Chen, J. 1996, AJ, 112, 1225
Jewitt, D. C., & Luu, J. X. 1995, AJ, 109, 1867
Jones, R. L., Gladman, B., Petit, J., et al. 2006, Icarus, 185, 508
Jones, R. L., Parker, J. W., Bieryla, A., et al. 2010, AJ, 139, 2249
Kavelaars, J. J., Jones, R. L., Gladman, B. J., et al. 2009, AJ, 137, 4917
Kobayashi, H., Ida, S., & Tanaka, H. 2005, Icarus, 177, 246
Levison, H. F., Morbidelli, A., Vanlaerhoven, C., Gomes, R., & Tsiganis, K. 2008, Icarus, 196, 258
Levison, H. F., & Stern, S. A. 1995, Icarus, 116, 315
LSST Science Collaborations, Abell, P. A., Allison, J., et al. 2009, arXiv:0912.0201
Lykawka, P. S., & Mukai, T. 2005, Planet. Space Sci., 53, 1175
Lykawka, P. S., & Mukai, T. 2007, Icarus, 189, 213
Malhotra, R. 1993, Nature, 365, 819
Malhotra, R. 1995, AJ, 110, 420
Malhotra, R. 1996, AJ, 111, 504
Melita, M. D., & Brunini, A. 2000, Icarus, 147, 205
Milani, A., Nobili, A. M., & Carpino, M. 1989, Icarus, 82, 200
Morais, M. H. M., & Morbidelli, A. 2002, Icarus, 160, 1
Morbidelli, A., Thomas, F., & Moons, M. 1995, Icarus, 118, 322
Murray-Clay, R. A., & Chiang, E. I. 2005, ApJ, 619, 623
Murray-Clay, R. A., & Schlichting, H. E. 2011, ApJ, 730, 132
Nagasawa, M., & Ida, S. 2000, AJ, 120, 3311
Nesvorný, D., & Dones, L. 2002, Icarus, 160, 271
Nesvorný, D., & Roig, F. 2000, Icarus, 148, 282
Nesvorný, D., & Roig, F. 2001, Icarus, 150, 104
Nesvorný, D., Roig, F., & Ferraz-Mello, S. 2000, AJ, 119, 953
Parker, A. H., & Kavelaars, J. J. 2010, ApJ, 722, L204
Petit, J., Kavelaars, J., Jones, R. L., et al. 2011, AJ, 142, 131
Sheppard, S. S., & Trujillo, C. A. 2010a, Science, 329, 1304
Sheppard, S. S., & Trujillo, C. A. 2010b, ApJ, 723, L233
Thomas, F., & Morbidelli, A. 1996, Celest. Mech. Dyn. Astron., 64, 209
Tiscareno, M. S., & Malhotra, R. 2009, AJ, 138, 827
Trujillo, C. A., Jewitt, D. C., & Luu, J. X. 2001, AJ, 122, 457
Volk, K., & Malhotra, R. 2008, ApJ, 687, 714
Wan, X., & Huang, T. 2007, MNRAS, 377, 133
Yeh, L., & Chang, H. 2009, Icarus, 204, 330